

## Article

# Hierarchical Auto-Ignition and Structure-Reactivity Trends of C<sub>2</sub>–C<sub>4</sub> 1-Alkenes

Wuchuan Sun <sup>1</sup>, Yingjia Zhang <sup>1,\*</sup>, Yang Li <sup>2</sup> and Zuohua Huang <sup>1</sup>

<sup>1</sup> State Key Laboratory of Multiphase Flows in Power Engineering, Xi'an Jiaotong University, Xi'an 710049, China; sunchuan@stu.xjtu.edu.cn (W.S.); zhhuang@xjtu.edu.cn (Z.H.)

<sup>2</sup> Science and Technology on Combustion, Internal Flow and Thermostructure Laboratory, School of Astronautics, Northwestern Polytechnical University, Xi'an 710072, China; yang.li@nwpu.edu.cn

\* Correspondence: yjzhang\_xjtu@xjtu.edu.cn; Tel.: +86-29-8266-5075; Fax: +86-29-8266-8789

**Abstract:** Ignition delay times of small alkenes are a valuable constraint for the refinement of the core kinetic mechanism of hydrocarbons used in representing combustion properties of real fuels. Moreover, the chemical reactivity comparison of those small alkenes provides a reference in object-oriented fuel design and logical combustion utilization. In this study, the ignition delay times of C<sub>2</sub>–C<sub>4</sub> alkenes (ethylene, propene and 1-butene) were measured behind reflected shock waves first, with a fixed oxygen concentration ( $X_{O_2} = 6\%$ ) and equivalence ratio ( $\varphi = 1.0$ ) at various pressures of 1.2, 4.0 and 16.0 atm, in order to facilitate the comparison. Three chemical-based-Arrhenius-type correlations covering a wide range of temperature, pressure, equivalence ratio, and dilution were proposed. The simplified reaction network for pyrolysis and oxidation of 1-alkenes was depicted relying on the reaction classes of alkenes. Nine generally accepted mechanisms were used to simulate the ignition delay times measured by this study as well as literature. All the kinetic models show reasonable structure-reactivity trends for all of the three alkenes, but only NUIGMech 1.1 is capable of representing quantitatively the chemical reactivity at all tested conditions. Generally, ethylene exhibits the highest reactivity while propene presents the lowest at high temperatures. Analyses of sensitivity and flux indicate that the main oxidation pathway of ethylene is chain-branching, which accelerates the accumulation of free radical pools, especially for the  $\dot{H}$  atom,  $\dot{O}$  atom and  $\dot{OH}$  radical, which results in the highest reactivity of ethylene. For propene and 1-butene, due to the presence of the allylic site, consumption of allylic radicals becomes the decisive step of oxidation and allylic radicals are mostly consumed by the  $\dot{H}O_2$  radical. However, there are no such efficient reaction pathways for the formation of  $\dot{H}O_2$  radicals during the propene oxidation process, while reaction pathways for  $\dot{H}O_2$  formation in 1-butene are efficient. Thus, 1-butene presents higher reactivity compared to propene.

**Keywords:** 1-alkenes; Arrhenius correlation; reactivity comparison; chemical kinetics



**Citation:** Sun, W.; Zhang, Y.; Li, Y.; Huang, Z. Hierarchical Auto-Ignition and Structure-Reactivity Trends of C<sub>2</sub>–C<sub>4</sub> 1-Alkenes. *Energies* **2021**, *14*, 5797. <https://doi.org/10.3390/en14185797>

Academic Editor: Giuseppe Pascazio

Received: 4 August 2021

Accepted: 8 September 2021

Published: 14 September 2021

**Publisher's Note:** MDPI stays neutral with regard to jurisdictional claims in published maps and institutional affiliations.



**Copyright:** © 2021 by the authors. Licensee MDPI, Basel, Switzerland. This article is an open access article distributed under the terms and conditions of the Creative Commons Attribution (CC BY) license (<https://creativecommons.org/licenses/by/4.0/>).

## 1. Introduction

An effective way to alleviate the demand growth for energy utilization and the corresponding deterioration of the atmospheric environment is to use the remaining fuels efficiently [1,2]. Computational fluid dynamic codes coupled with detailed or reduced combustion mechanisms are powerful approaches in helping researchers to improve combustor performance in increasing efficiency and reducing pollutant emission. Many studies have been therefore devoted to developing accurate combustion kinetic mechanisms for conventional fuels [3–5], including methane, ethane, propane, butane, as well as renewable fuels, such as alcohols [6,7] and esters [8,9]. With the combustion mechanisms of these fuels being mature, more effort is now being focused on stable intermediate species produced in combustion processes [10], especially the products which could cause detrimental effects on the atmospheric environment.

Alkenes not only dominate the formation of soot and polycyclic aromatic hydrocarbons (PAHs) [11], but also are critical intermediate species in the pyrolysis and oxidation of normal alkanes as well as bio-fuels [12]. Most importantly, the combustion mechanisms of alkenes constitute a critical element for hydrocarbon fuels. It is therefore imperative to fully understand the combustion fundamentals of alkenes; ignition delay times (IDTs), for instance, are a required and extensively used parameter for validation and refinement of kinetic mechanisms.

1-alkenes have been extensively studied due to the simpler structure and an important precursor for soot formation. 1-alkenes are readily formed via the  $\beta$ -scission reaction of alkyl radicals in the combustion or pyrolysis of larger hydrocarbons. Many works have been done with auto-ignition characteristics and chemical kinetic model of ethylene [4,13–33], propene [34–41] and 1-butene [36,42,43]. In spite of the IDTs of C<sub>2</sub>–C<sub>4</sub> alkenes have been reported diversely, it remains difficult to compare straightforward the literature data due to different conditions, diverse facilities and various definitions of IDTs. It is not necessarily surprising that there is a lack of comprehensive comparison of structure-reactivity for 1-alkenes in this way. Kukui et al. [44] investigated the ignition and combustion characteristics of weak flames for ethylene, propylene, 1-butene and 1-pentene in a micro flow reactor. The reactivity of the four alkenes was proposed to be in order of ethylene, 1-pentene, 1-butene and propene, from high to low. The highest reactivity of ethylene comes from a higher rate of production of  $\dot{O}H$  through faster  $\dot{H}O_2$  accumulation via the reaction sequence  $\dot{H}CO + O_2 = CO + \dot{H}O_2$ ,  $\dot{C}_2H_5 + O_2 = C_2H_4 + \dot{H}O_2$  and  $\dot{C}_2H_3 + O_2 = C_2H_2 + \dot{H}O_2$ , in the initial oxidation stage. Li et al. [45] compared the IDTs of butene isomers measured by both shock tube (ST) and rapid compression machine (RCM). Results reveal that 1-butene is the fastest, followed by 2-butene, with isobutene being the slowest. Shao et al. [27] measured IDTs of methane, ethylene, propene and their blends in 4% O<sub>2</sub>, balance Ar mixtures, over the temperature range of 950–1800 K, at pressures of 14–60 atm and equivalence ratios of one and two. Their work mainly focuses on extending the conditions of previous studies to higher pressures, and provides a uniform set of kinetics for the evaluation of core mechanisms. Jach et al. [46] collected extensive IDTs of C<sub>2</sub>–C<sub>6</sub> alkenes and acetylene. They assessed the performance of 15 detailed kinetic mechanisms and provided guidance for the mechanism selection.

Recently, Nagaraja et al. [47] investigated hierarchically the pyrolysis of C<sub>2</sub>–C<sub>6</sub> 1-alkenes at 2 bar in the temperature range of 900–1800 K using a single-pulse shock tube and made a contribution to the database for mechanism validation and reactivity comparison. Dong et al. [29] performed a comparative comparison study on the reactivity of 1-alkenes from ethylene to 1-heptene at an equivalence ratio of 1.0, at a pressure of 30 atm in the temperature range of 600–1300 K. Their results illustrate that 1-alkenes with longer carbon chains have higher fuel reactivity at low temperatures. At high temperatures, however, all of the fuels show quite similar fuel reactivity, except propene with remarkably longer IDTs.

As stated above, the studies of IDTs for 1-alkenes are diversiform. There are however few relevant inspections both systematic and with the same external conditions. This work presents a comprehensive review on auto-ignition behaviors and combustion chemistry of three small 1-alkenes (ethylene, propene and 1-butene). As a prerequisite and background for the necessity of detailed combustion chemistry research, this work begins by providing the chemical kinetics of 1-alkenes, thus important reaction channels in the pyrolysis and oxidation of 1-alkenes are highlighted. Subsequently, the IDTs of the three 1-alkenes are used to assess the performance of literature kinetic mechanisms. Chemical-based Arrhenius correlations are proposed for engineering applications. Finally, a hierarchical reactivity comparison of the three 1-alkenes is implemented experimentally and theoretically. This work closes by summarizing distinguishing characteristics of alkenes combustion chemistry and prospecting future research in this area.

## 2. Experimental Details

All measurements were carried out using a stainless steel shock tube which has already been described in our previous work [48]. Briefly, the shock tube has an internal diameter of 11.5 cm, divided into a 4 m long driver section and a 4.8 m long driven section. High purity helium (99.999%) was used as the driver gas. PET (polyethylene terephthalate) diaphragms with different thicknesses varying from 0.025 to 0.4 mm were assembled to obtain desired reflected shock pressure. Before each experiment, the shock tube was evacuated to 1.0 Pa with a leaking rate of 1.0 Pa/min by a mechanical-roots combined pump system. Fuel mixtures were prepared in a 128 L stainless steel vessel and allowed to rest for more than 12 h to ensure sufficient diffusion and mixing. The partial pressure of each composition was measured with a high-accuracy pressure transmitter (ROSEMOUNT 3051). Table 1 provides a list of the fuel compositions tested in this study. The fuel purities were 99.99%, and the purities of oxygen and argon were 99.999%.

**Table 1.** Composition of the fuel mixtures tested in this study.

Mixture	Fuel	X <sub>fuel</sub> (%)	X <sub>O<sub>2</sub></sub> (%)	X <sub>AR</sub> (%)
1	ethylene	2.0	6	92.0
2	propene	1.33	6	92.67
2	1-butene	1.0	6	93.0

Three time counters (FLUKE PM6690) were triggered by four pressure transducers (PCB 113B26) installed in the last 1.3 m of the shock tube with an equal-distance of 300 mm. Recorded time intervals were used to calculate incident shock velocity, which was extrapolated to the end wall to determine reflected shock temperature ( $T_5$ ) using a chemical equilibrium program Gaseq [49]. Reflected-shock pressure ( $p_5$ ) was monitored using a pressure transducer (PCB, 113B03) with pressure compensation. Both OH\* light emission detected by a photomultiplier (HAMAMATSU, CR131) with a narrow filter centered at  $307 \pm 10$  nm and inherently large pressure rise was used to verify ignition event. The IDT was defined as the time interval between the vertical rise in pressure and the extrapolation of the steepest rise of excited OH\* emission to the zero line, as depicted in Figure 1. The typical uncertainty in the reflected shock temperature is  $\pm 20$  K using the standard root-sum-square (RSS) method [50–52].

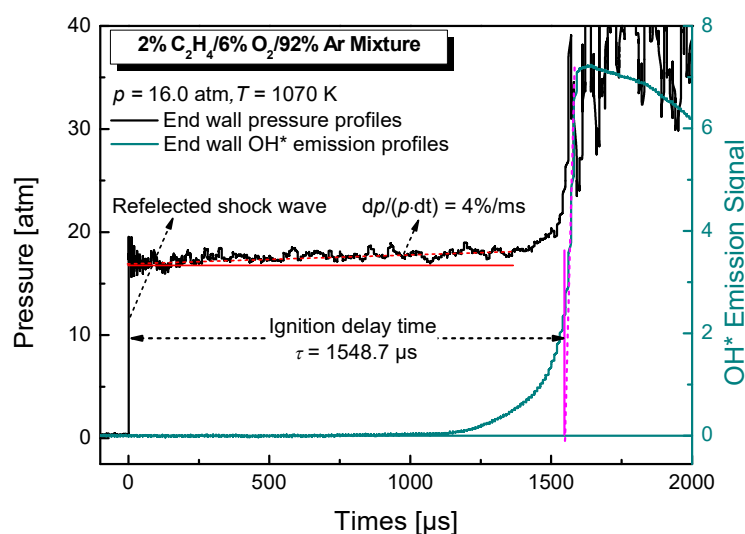


**Figure 1.** Typical end wall pressure and OH\* time-history used to determine the ignition delay time.

Simulations of the IDTs were carried out using the 0-D homogeneous closed reactor of Chemkin-Pro software [53]. Similar to our previous study [48,54], a typical pressure rise rate

of 4%/ms was observed and have been included in the calculations with SENKIN/VTIM approach [55] for considering the non-ideal effect. The calculated IDT was defined as the time interval from the beginning of the simulation to the maximum rate of temperature rise (i.e.,  $\max dT/dt$ ), which has been demonstrated to be consistent with this measurement.

### 3. Hierarchical Kinetics of 1-Alkenes

#### 3.1. Comparison of Chemical Bond Energy

The access to distinguish fuel reactivity is to explore structural features of fuel molecules which affect molecular level transformations during combustion. Alkenes are unsaturated hydrocarbons with at least one C=C double bond resulting in prominent differences in thermodynamics and reaction kinetics properties relative to saturated alkanes.

Molecular structures and bond dissociation energies (BDEs) of ethylene, propene and 1-butene at room temperature are depicted in Figure 2. Starting from the alkene-specific moiety, allylic C–C and C–H bonds show relatively weaker BDE with the range of 75.22–87.57 kcal/mol (highlighted in red), thus reactions are predictable to be the most favorable to proceed via the allylic bond fission. In contrast, vinylic C–H bonds have relatively stronger BDEs with the range of 106.96–111.74 kcal/mol. The cause for the different BDEs of allylic and vinylic sites comes mainly from electron delocalization, where allylic carbons share a pair of  $\pi$  electrons, results in initial H-atom abstractions more readily in order of allylic C–H, methyl C–H and vinylic C–H sides.

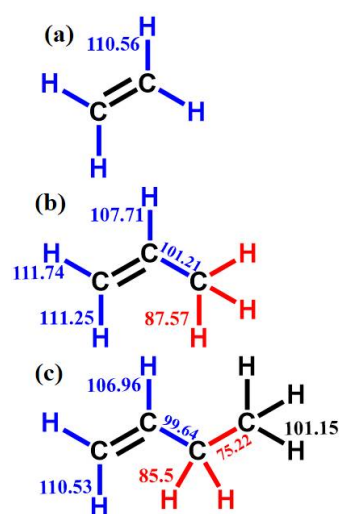


**Figure 2.** Molecular structure and BDEs of ethylene (a), propene (b) and 1-butene (c) at 298.15 K. The BDEs of ethylene, propene and C–C bonds in 1-butene were adopted from the ATcT database [56] while the C–H bonds in 1-butene were taken from Li et al. [43].

#### 3.2. Reaction Scheme for Pyrolysis and Oxidation of 1-Alkenes

The reaction subsets for pyrolysis and oxidation of alkenes have been developed previously [4,32,36,38,39,43]. According to the hierarchical rate rule of reaction classes, we summarized the general reaction scheme of 1-alkenes, Figure 3.

##### 3.2.1. Unimolecular Reactions

Dominant unimolecular reactions include simple C–C and C–H bond fission reactions, which are crucial to accurately describe high-temperature pyrolysis and oxidation of 1-alkenes. For ethylene, vinylic C–H bond fission reaction is the preferred channel. For propene, the allylic C–H bond fission reaction channel is more competitive. When the carbon number is greater than three, the allylic C–C bond fission becomes more favorable due to the lowest BDE.

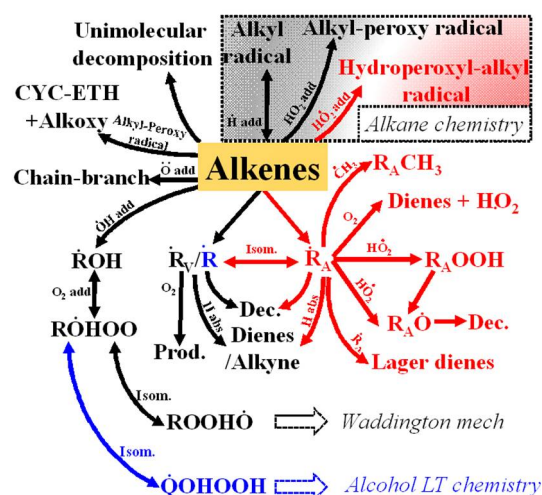


**Figure 3.** Simplified reaction scheme for pyrolysis and oxidation of 1-alkenes. (Black: all 1-alkenes, red: 1-alkenes with carbon number >2 and blue: 1-alkenes with carbon number >3).

### 3.2.2. H-Atom Abstraction Reactions

H-atom abstraction reactions (H-abs) are the primary means in fuel oxidation via a variety of small fragments ( $\dot{\text{H}}$ ,  $\dot{\text{O}}$ ,  $\dot{\text{O}}\text{H}$ ,  $\text{H}\dot{\text{O}}_2$ ,  $\dot{\text{C}}\text{H}_3$ ,  $\text{O}_2$ ) attack. The most important fragment is the  $\dot{\text{O}}\text{H}$  radical, due in part to the exothermicity of water formation.  $\text{H}\dot{\text{O}}_2$  radical is also important at high pressure and intermediate temperature owing to the formation of  $\text{H}_2\text{O}_2$  which is a chain branching carrier and enriches free radical pools. Besides, H-abs by  $\text{O}_2$  reaction promotes reactivity due to its chain branching characteristics.

There are four different types of H-abs reactions in 1-alkenes, and they obey an order of priority of allylic C–H site > secondary C–H site > primary C–H site > vinylic C–H site. All 1-alkenes can undergo H-abs reactions on vinylic C–H site with vinyl radicals ( $\text{R}_\text{V}$ ) formation, while H-abs reactions on allylic C–H site with allyl radicals ( $\text{R}_\text{A}$ ) formation, as well as primary and secondary C–H sites with alkenyl radicals ( $\text{R}$ ) formation can only occur on 1-alkenes with carbon numbers larger than 2, 3 and 4, respectively. Among them, H-abs reactions on allylic C–H sites by  $\dot{\text{O}}\text{H}$  radicals is the most inhibiting reaction because resonantly stabilized allylic radicals generate more reactive  $\dot{\text{O}}\text{H}$  radical scavengers. The allylic radicals formed readily either re-combine to form stable dienes or react with methyl radical to yield larger alkenes.

### 3.2.3. Fuel Radical Reactions

Fuel radicals ( $\text{R}_\text{V}$ ,  $\text{R}_\text{A}$  and  $\text{R}$ ) can continue to decompose into smaller radicals following the  $\beta$ -scission and H-abs reaction to form dienes and alkynes.  $\text{R}_\text{V}$  and  $\text{R}$  radicals also can be consumed by reacting with oxygen molecules. The consumption of  $\text{R}_\text{A}$  is important, and the reaction of allyl radicals with molecular oxygen promotes reactivity because the low reactive stabilized allylic radical converts to a more reactive hydroperoxyl radical. The reactions of allyl radicals with  $\text{H}\dot{\text{O}}_2$  forming allylic hydroperoxide radicals and allyloxy radicals are also an important class across a range of conditions, especially at low to intermediate temperatures due to  $\dot{\text{O}}\text{H}$  radicals being generated directly or subsequently decomposed by hydroperoxides.

### 3.2.4. Radical Addition Reactions

Precisely because of the proper C=C double bond in alkenes, more diverse reactions such as radical addition reactions can occur relative to alkanes. In addition to hydroxyl radicals forming, an alcohol radical promotes reactivity at low-temperatures. The underlying kinetic mechanism is that chain branching can subsequently occur through alcohol low-temperature pathways via alcohol radicals adduct to  $\text{O}_2$ ; these form hydroxyalkyl-peroxy radicals, internal H-atom isomerization with the formation of hydroxyalkyl hydroperoxide

radicals, the second addition to O<sub>2</sub>, with the decomposition of the newly formed keto-hydroperoxide species eventually promoting reactivity through generation of hydroxyl radicals. These reaction channels occur more easily in alkenes with at least four carbons, because these alkenes are more likely to abstract the H atom from the C–H site to form hydroxyalkyl hydroperoxide via the internal H-atom isomerization process described above. Moreover, the hydroxyalkyl-peroxyl radicals can also undergo Waddington-type reaction pathways via a six-membered ring transition state (TS) to abstract a H atom from hydroxyl moiety, followed by decomposition to produce an OH radical and two aldehydes. This chain propagating process directly competes with the alkyl-type low-temperature chain branching channels, thus inhibiting the reactivity.

In addition, the reaction flux overlaps with alkane chemistry when alkyl radical formed via H atom addition and alkyl-peroxyl radical or hydroperoxyl-alkyl radical generated via HO<sub>2</sub> addition. H-atom addition inhibits reactivity at high and intermediate temperatures, due to the competition with chain branching reaction  $\dot{H} + O_2 = \ddot{O} + \dot{OH}$ . It is however a promoting reaction at low temperature as going to alkyl-like chemistry via first and second O<sub>2</sub> additions.

#### 4. Ignition Delay Times of C<sub>2</sub>–C<sub>4</sub> 1-Alkenes

The summary of the experimental conditions given in Table 2 provides an overview of the auto-ignition studies of ethylene, propene and 1-butene. The list includes data acquired for pure, gaseous combustion of the respective alkene under well-defined conditions. Accompanying the graph is plots representing the approximate range of equivalence ratios (*x*-axis), pressures (*y*-axis), and temperatures (color maps) where the IDTs of alkenes have been measured, while the grey area represents no data under such conditions in Figure 4.

The early articles reporting alkene auto-ignition can date back to the 1970s. Among those works, ethylene is the most favorably studied due to its practical application potentiality and as the base work of developing alkene kinetic models. Auto-ignition characteristics of ethylene are included, with various thermal boundary conditions covering temperature (720–2240 K), pressure (1–60 atm), equivalent ratio (0.3–3.0) and diluted gas. However, experimental data for ethylene/air mixtures remains lacking, especially at high pressures exceeding 25 atm, (Figure 4(a<sub>2</sub>)). There are fewer studies on propene and 1-butene, but both of them cover high to low temperatures and engine relevant conditions, (Figure 4(b<sub>2</sub>,c<sub>2</sub>)). Regarding propene, the IDTs are still rare at pressures from 10–30 atm for fuel-rich mixtures, (Figure 4(b<sub>2</sub>)). For 1-butene, the high-pressure experimental data of diluted gas are scarce especially at pressures up to 16 atm, and they are important to verify chemical kinetic models. Besides, for all three alkenes, there are no IDTs data below atmospheric pressures.

The collected experimental data of C<sub>2</sub>–C<sub>4</sub> 1-alkenes do not show negative temperature coefficient (NTC) behavior, as shown in Supplementary Materials. The above chemical kinetic analysis indicates that possible reasons for 1-alkenes NTC behavior are generally originated from reaction pathways flowing into the alcohol low-temperature mechanism. Specifically, at lower temperatures, the fuel-OH reaction branch shifts to addition reactions with hydroxyalkyl radicals producing. Subsequently, the chain branching occurs via hydroxyalkyl radicals addition to O<sub>2</sub>, internal H-atom isomerization, the second addition to O<sub>2</sub>, with the decomposition of the newly formed ketohydroperoxide species eventually promoting reactivity through OH generation. Regarding 1-butene, during the inter H-atom isomerization step, 1,5 H-shift reaction of the C<sub>4</sub>H<sub>8</sub>OH1-2O<sub>2</sub> radical leading to chain branching occurs more arduously than 1,4 H-shift reaction, as a result of the weaker C-H bonds by presence of hydroxyl group. Thus, 1-butene shows no NTC behavior as less fuel flux proceeds from the low-temperature mechanism. Propene and ethylene do not show NTC behavior either, because hydroxyalkyl-peroxyl radicals have no chance to undergo chain branching reaction pathways due to less carbon chain length.

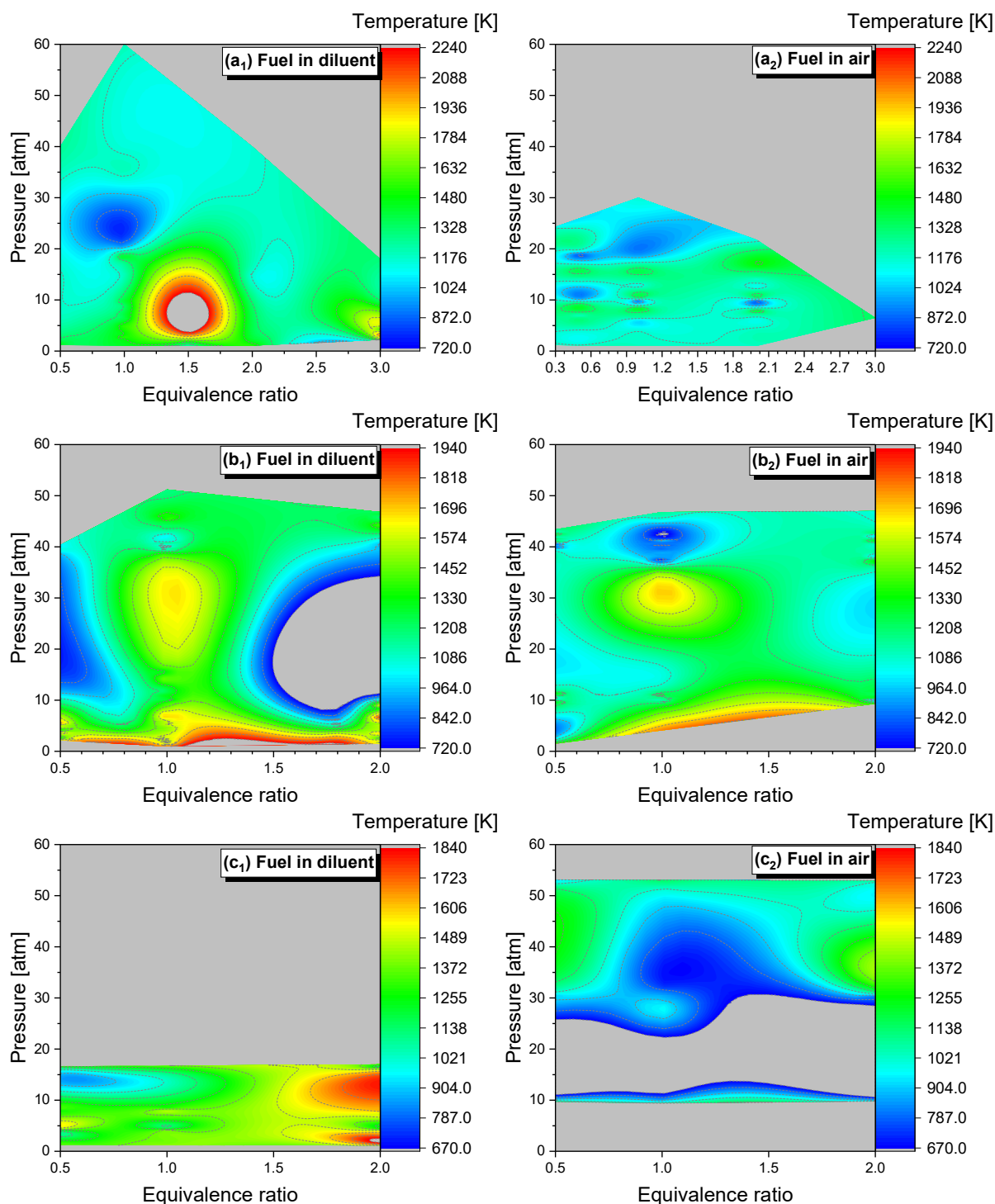


**Figure 4.** Three-dimensional plots representing the approximate range of temperatures, pressure and equivalence ratios at which alkene IDTs have been studied. (a<sub>1</sub>)/(a<sub>2</sub>) ethylene, (b<sub>1</sub>)/(b<sub>2</sub>) propene, (c<sub>1</sub>)/(c<sub>2</sub>) 1-butene.

Table 2. Ignition delay time studies of C<sub>2</sub>–C<sub>4</sub> 1-alkenes.

Experimental Device			Experimental Conditions						Ref.
Type	Diameter (cm)	Diagnostic	Mixture	Dilution	$\varphi$	T (K)	p (atm)	IDT (us) Range	
ST	4.3	CH* onset at sidewall	C <sub>2</sub> H <sub>4</sub> /O <sub>2</sub> /Ar	96%	1.0	1422–2042	1.77–3.12	<108	Hidaka et al. [13]
				97%	1.5	1469–2081	1.86–3.12	<152	
				98%	3.0	1596–2077	2.42–5.00	<62	
ST	7.6 × 3.8 cross section	CH* onset at endwall	C <sub>2</sub> H <sub>4</sub> /O <sub>2</sub> /Ar	75%/96%	1.0	1102–2236	1.26–4.09	<765.44	Brown and Thomas [14]
			C <sub>2</sub> H <sub>4</sub> /O <sub>2</sub> /N <sub>2</sub>	75%	1.0	1073–1566	2.22–4.74	<755.82	
ST	15.24	d[CH*]/dt max at endwall	C <sub>2</sub> H <sub>4</sub> /O <sub>2</sub> /Ar	84%/92%/96%	1.0	1253–1572	1,2 and 4	<248	Horning et al. [15]
ST	3.8	OH* onset at sidewall	C <sub>2</sub> H <sub>4</sub> /O <sub>2</sub> /Ar	95.10%	0.5	1125–1308	4.83–7.89	<948	Collect and Spadaccini [16]
				96.50%	0.75	1182–1350	5.76–7.53	<524	
				97.20%	1.0	1380–1414	6.58–7.64	<136	
ST	16.2	d[OH*]/dt max at endwall	C <sub>2</sub> H <sub>4</sub> /O <sub>2</sub> /Ar	96%/98%	1.0	1223–1746	0.9–3.3	<1780	Kalitan et al. [17]
				96%/98%	0.5	1115–1754	1–1.38	<3397	
ST	5.08	CH*/OH* onset, Visibel light at endwall	C <sub>2</sub> H <sub>4</sub> /O <sub>2</sub> /Ar	93%/96%/98%	1.0	1034–1828	2,10 and 18	<4200	Saxena et al. [21]
				93%	3.0	1000–1592	2,10 and 18	<4404	
ST	15.24	d[CH*]/dt max at endwall	C <sub>2</sub> H <sub>4</sub> /O <sub>2</sub> /Ar	95.33%	0.5	1113–1244	15	<1708	Davidson et al. [22]
				94.67%	1.0	1130–1267	15,35	<1119	
				93.33%	2.0	1099–1216	15	<1325	
ST	15.24	d[OH*]/dt max at sidewall	C <sub>2</sub> H <sub>4</sub> /O <sub>2</sub> /Ar	98%	0.5, 1.0 and 2.0	1181–1808	0.9 and 1.7	<1512	Mathieu et al. [25]
ST	7.5	d[CH*]/dt max at sidewall	C <sub>2</sub> H <sub>4</sub> /O <sub>2</sub> Ar	75% and 96%	1.0	1092–1743	1.3–3.0	<3257	Xiong et al. [26]
ST	5(diver insert)	dp/dt max and d[OH*]/dt max at sidewall	C <sub>2</sub> H <sub>4</sub> /O <sub>2</sub> /Ar	94.73%	1.0	1090–1317	16 and 60	<1120	Shao et al. [27]
				93.39%	2.0	1122–1268	16	<1070	
ST	7.5	d[CH*]/dt max at sidewall	C <sub>2</sub> H <sub>4</sub> /O <sub>2</sub> /Ar	94.92%	1.0	1132–1745	2	<1679	Xiong et al. [31]
			C <sub>2</sub> H <sub>4</sub> /O <sub>2</sub> /Ar/N <sub>2</sub>	(75.94%AR+ 18.98%N2)	1.0	1074–1710	2	<2467	
ST	6.35	dp/dt max at end wall and d[OH*]/dt max at sidewall	C <sub>2</sub> H <sub>4</sub> /O <sub>2</sub> /Ar	90%	0.5	1017–1503	40	<2258	Baigmohammadi et al. [28]
				75%	1.0	987–1113	20	<1782	
				85%	1.0	998–1349	40	<1620	
				75%	2.0	945–1349	40	<1686	

Table 2. Cont.

Experimental Device			Experimental Conditions						Ref.
Type	Diameter (cm)	Diagnostic	Mixture	Dilution	$\varphi$	$T$ (K)	$p$ (atm)	IDT (us) Range	
ST	3.8	$p$ increased by 10% at sidewall	C <sub>2</sub> H <sub>4</sub> /O <sub>2</sub> /Ar	Ar=N <sub>2</sub> in air	0.33,1.0 and 3.0	1090–1520	6.5	<318	Tereza et al. [20]
ST	7.6	CH/OH/C <sub>2</sub> /p onset at end wall	C <sub>2</sub> H <sub>4</sub> /Air	/	0.5,1.0 and 2.0	1060–1520	5.9–16.5	<1112	Penyazkov et al. [19]
ST	16.2/15.24	dp/dt max at sidewall	C <sub>2</sub> H <sub>4</sub> /Air	/	0.3,0.5,1.0 and 2.0	1003–1401	1.0–24.9	<2228	Kopp et al. [23]
ST	10	d[CH*]/dt max at sidewall	C <sub>2</sub> H <sub>4</sub> /Air	/	0.5,1.0 and 2.0	721–1320	1, 4, 10 and 19	<8664	Yang et al. [32]
ST	6.3	dp/dt max at endwall	C <sub>2</sub> H <sub>4</sub> /Air	/	1.0	1055–1250	30	<500	Dong et al. [29]
RCM	/	dp/dt max	C <sub>2</sub> H <sub>4</sub> /O <sub>2</sub> /Ar/N <sub>2</sub>	89.429%(15.856%N <sub>2</sub> , 73.573%Ar)	1.0	850–1050	15, 30 and 50	572–273,000	Kumar et al. [18]
RCM	/	dp/dt max	C <sub>2</sub> H <sub>4</sub> /O <sub>2</sub> /Ar/N <sub>2</sub>	85%(48%N <sub>2</sub> ,37%Ar)	0.5	915–1008	20	4748–142,200	Baigmohammadi et al. [28]
				85%(75%N <sub>2</sub> ,15%Ar)	0.5	882–958	40	9700–92,250	
				75%(30%N <sub>2</sub> ,45%Ar)	1.0	886–947	20	8443–87,890	
				85%(55%N <sub>2</sub> ,30%Ar)	1.0	838–935	40	10,700–191,000	
				90%(45%N <sub>2</sub> ,45%Ar)	2.0	881–980	20	10,230–418,900	
RCM	/	dp/dt max	C <sub>2</sub> H <sub>4</sub> /O <sub>2</sub> /"Air"	"Air"(16.93%O <sub>2</sub> ,40%Ar,33.83N <sub>2</sub> )	1.0	800–920	30	7196–310,000	Dong et al. [29]
ST	5.4	$p$ onset at endwall	C <sub>3</sub> H <sub>6</sub> /O <sub>2</sub> /Ar	84% and 92%	0.5	1272–1772	≈4	<932	Burcat and Radhakrishnan [34]
				91.2% and 96.7%	1	1366–1725	2.19–6.473	<922	
				94.8% and 89.6%	2	1443–1936	4.19–7.018	<737	
ST	7.62	dp/dt max at endwall	C <sub>3</sub> H <sub>6</sub> /O <sub>2</sub> /Ar	84% and 92%	0.5	1270–1705	3.89	<1535	Qin et al. [35]
				82.10%	0.8	1285–1505	3.71	<1260	
				91.20%	1	1530–1820	1.14	<265	
				89%	1.8	1320–1565	3.92	<1285	
				94.80%	2	1415–1770	4.05	<1305	

Table 2. Cont.

Experimental Device			Experimental Conditions						Ref.	
Type	Diameter (cm)	Diagnostic	Mixture	Dilution	$\varphi$	T (K)	p (atm)	IDT (us) Range		
ST	6.35	$dp/dt$ max at sidewall	C <sub>3</sub> H <sub>6</sub> /O <sub>2</sub> /Ar	95.11%	1	1175–1500	40	<1754	Burke et al. [39]	
ST	15.2	$dp/dt$ max at end endwall or d[OH*]/dt max at sidewall	C <sub>3</sub> H <sub>6</sub> /O <sub>2</sub> /Ar	85.33% and 95.11%	1	1222–1645	2 and 10	<2046		
ST	5.7	d[OH*]/dt max at endwall	C <sub>3</sub> H <sub>6</sub> /O <sub>2</sub> /Ar C <sub>3</sub> H <sub>6</sub> /O <sub>2</sub> /N <sub>2</sub>	94.22% 85.33%	2 1	1313–1714 1220–1462	2 and 10 10	<2096 <1476		
ST	14.13/15.34	d[OH*]/dt max at endwall	C <sub>3</sub> H <sub>6</sub> /O <sub>2</sub> /Ar	85.33% 95.55%	1 0.5	1253–1422 1360–1689	10 2	<1059 <2002		
ST	5 (diver insert)	d[OH*]/dt max at endwall	C <sub>3</sub> H <sub>6</sub> /O <sub>2</sub> /Ar	91.13% and 95.11%	1	1333–1720	2 and 4.5	<2472		
ST	5 (diver insert)	d[OH*]/dt max at endwall	C <sub>3</sub> H <sub>6</sub> /O <sub>2</sub> /Ar	94.22% 95.11%	2 1	1388–1756 1195–1302	2 40	<2324 <1877		
ST	5 (diver insert)	d[OH*]/dt max at endwall	C <sub>3</sub> H <sub>6</sub> /O <sub>2</sub> /Ar	94.22%	2	1200–1432	40	<1543		
ST	5 (diver insert)	$dp/dt$ max and d[OH*]/dt max at sidewall	C <sub>3</sub> H <sub>6</sub> /O <sub>2</sub> /Ar	95.16%	1	1255–1488	15.11	<3022		Shao et al. [27]
ST	6.35	$dp/dt$ max at sidewall	C <sub>3</sub> H <sub>6</sub> /Air	/	0.5 and 1.0	1106–1364	10	<1736		Burke et al. [39]
ST	15.2	$dp/dt$ max at end endwall or d[OH*]/dt max at sidewall	C <sub>3</sub> H <sub>6</sub> /Air	/	0.5 and 1.0	1112–1535	2 and 10	<1660		
ST	5.7	d[OH*]/dt max at endwall	C <sub>3</sub> H <sub>6</sub> /Air	/	0.5, 1.0 and 2.0	1036–1406	10 and 40	<1642		
ST	10	p/OH* onset at both sidewall and endwall	C <sub>3</sub> H <sub>6</sub> /Air	/	0.5, 1.0 and 2.0	1024–1332	40	<1319		
RCM	/	$dp/dt$ max	C <sub>3</sub> H <sub>6</sub> //Air	/	0.5 and 1.0	722–1108	10 and 40	2000–325,000	Burke et al. [39]	
			C <sub>3</sub> H <sub>6</sub> /O <sub>2</sub> /Ar	95.55%	0.5	941–1220	10 and 40	5800–212,000		
			C <sub>3</sub> H <sub>6</sub> /O <sub>2</sub> /Ar/N <sub>2</sub>	95.11%(47.555%Ar, 47.555%N <sub>2</sub> )	1	1109–1238	10	9517–162,800		
			C <sub>3</sub> H <sub>6</sub> /O <sub>2</sub> /N <sub>2</sub>	95.11%	1	898–1008	40	20,000–146,700		
			C <sub>3</sub> H <sub>6</sub> /O <sub>2</sub> /Ar/N <sub>2</sub>	85.33%(21.33%Ar, 64%N <sub>2</sub> )	1	988–1129	10	6450–128,000		
			C <sub>3</sub> H <sub>6</sub> /O <sub>2</sub> /Ar	85.33%	1	781–957	40	6225–296,700		
			C <sub>3</sub> H <sub>6</sub> //Air'	Air'(21O <sub>2</sub> :37.5 AR:37.5N <sub>2</sub> )	1 and 2	859–1009	10	10,220–157,200		
RCM	/	$dp/dt$ max	C <sub>3</sub> H <sub>6</sub> /O <sub>2</sub> /Ar/N <sub>2</sub>	85.33%(42.665%Ar, 42.665%N <sub>2</sub> )	1	813–1062	10 and 40	9900–105,740		
			C <sub>3</sub> H <sub>6</sub> /O <sub>2</sub> /Ar/N <sub>2</sub>	94.22%(47.11%Ar, 47.11%N <sub>2</sub> )	2	892–1178	10 and 40	12,000–114,560		
			C <sub>3</sub> H <sub>6</sub> /O <sub>2</sub> /N <sub>2</sub>	95.11%	1	912–1021	40	15,900–80,500		

Table 2. Cont.

Experimental Device			Experimental Conditions						Ref.
Type	Diameter (cm)	Diagnostic	Mixture	Dilution	$\varphi$	$T$ (K)	$p$ (atm)	IDT (us) Range	
ST	7.8	OH* increased by 10% at sidewall	C <sub>4</sub> H <sub>8</sub> -1/O <sub>2</sub> /Ar	87% and 93% 96%	0.5	1248–1538	~7.89	<932	Heyberger et al. [36]
					1	1202–1568	~7.94	<1907	
					2	1442–1664	~7.44	<148	
ST	11.5	d[OH*]/dt max at endwall	C <sub>4</sub> H <sub>8</sub> -1/O <sub>2</sub> /Ar	87% 94.75% and 96.5% 96%	0.5	974–1585	1.2, 4.0 and 16.0	<3948	Pan et al. [42]
					1	1142–1705	4	<3431	
					2	1082–1835	1.2, 4.0 and 16.0	<3518	
ST	6.35	dp/dt max at endwall	C <sub>4</sub> H <sub>8</sub> -1/Air	/	0.5	929–1289	10, 30 and 50	<2008	Li et al. [43]
					1	940–1285	10, 30 and 50	<1945	
					2	899–1301	10, 30 and 50	<1960	
RCM	/	dp/dt max	C <sub>4</sub> H <sub>8</sub> -1/Air	/	0.5	765–1012	10 and 30	<92,290	
					1	688–941	10 and 30	<231,700	
					2	676–940	10 and 30	<201,500	

#### 4.1. Model Performance Comparison

A number of kinetic mechanisms of ethylene, propene and 1-butene are available in the literature. It is costly to cover all of those kinetic mechanisms, thus only some generally accepted mechanisms published in recent years are listed (Table 3) to inspect their performance in terms of predicting IDTs presented in Table 2. Figures 5–9 compare the IDTs of C<sub>2</sub>–C<sub>4</sub> alkenes measured in this study to the model simulations with nine selected kinetic mechanisms. Additional comparisons with the literature data are available in the Supplementary Materials.

Table 3. Summary of mechanism selected in this study.

Mechanism	No. of Species	No. of Reactions	Application of Present	Year of Released	Ref
NUIGMech 1.1	2845	112,60	C <sub>2</sub> –C <sub>4</sub>	2021	[29,47,57–63]
AramcoMech 2.0	493	2716	C <sub>2</sub> –C <sub>4</sub>	2013	[4,6,38,39,45,64,65]
Creck	621	27,369	C <sub>2</sub> –C <sub>4</sub>	2020	[3,66,67]
UCSD	55	245	C <sub>2</sub> –C <sub>4</sub>	2016	[68]
Jetsurf 2.0	344	2163	C <sub>2</sub> –C <sub>4</sub>	2010	[69]
Konnov 0.6	131	1256	C <sub>2</sub> –C <sub>4</sub>	2009	[70]
USC 2.0	113	809	C <sub>2</sub> –C <sub>4</sub>	2007	[71]
ChuanDa	146	567	C <sub>2</sub>	2020	[32]
Glarborg 2009	118	987	C <sub>2</sub>	2009	[72]

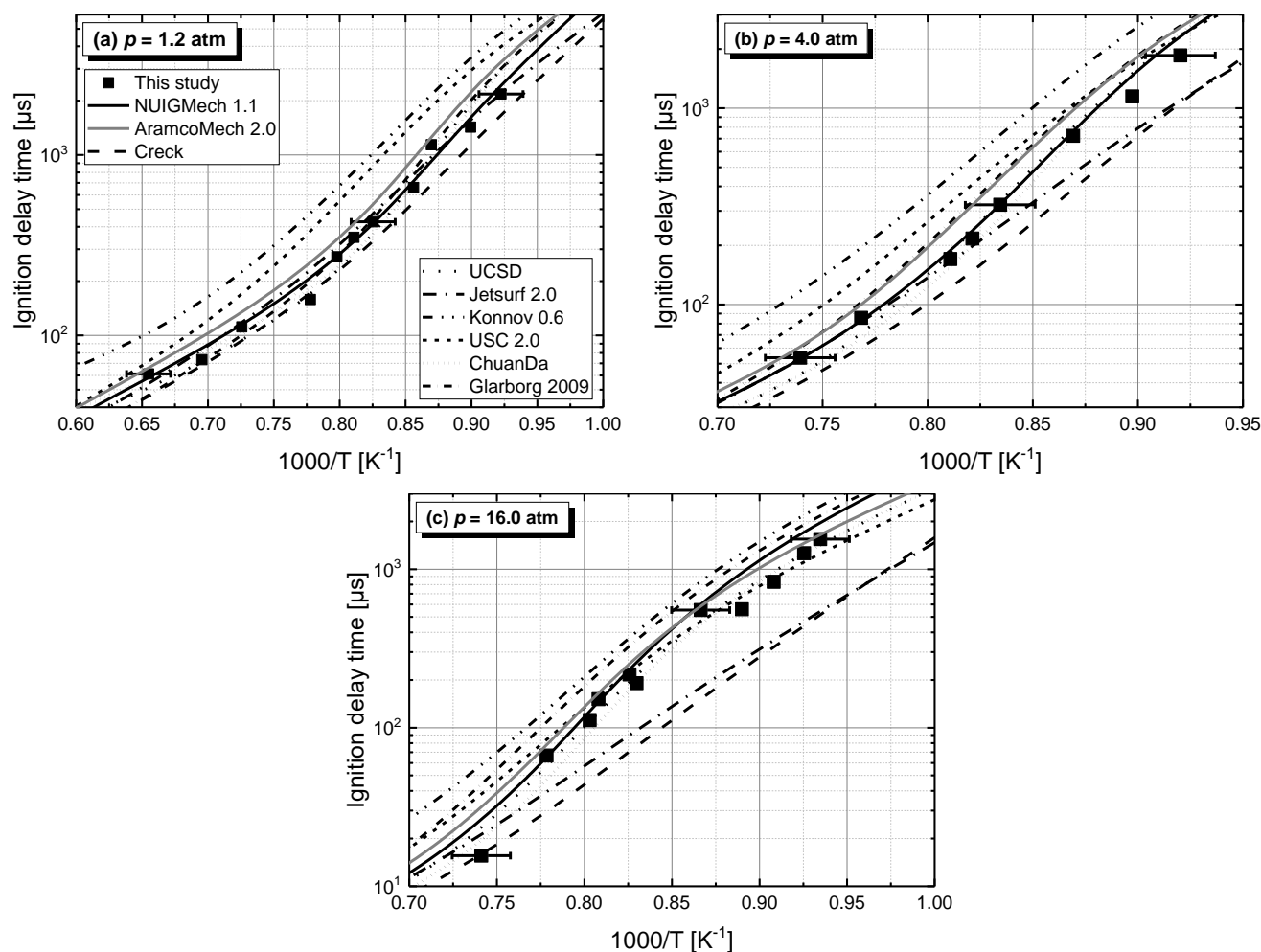
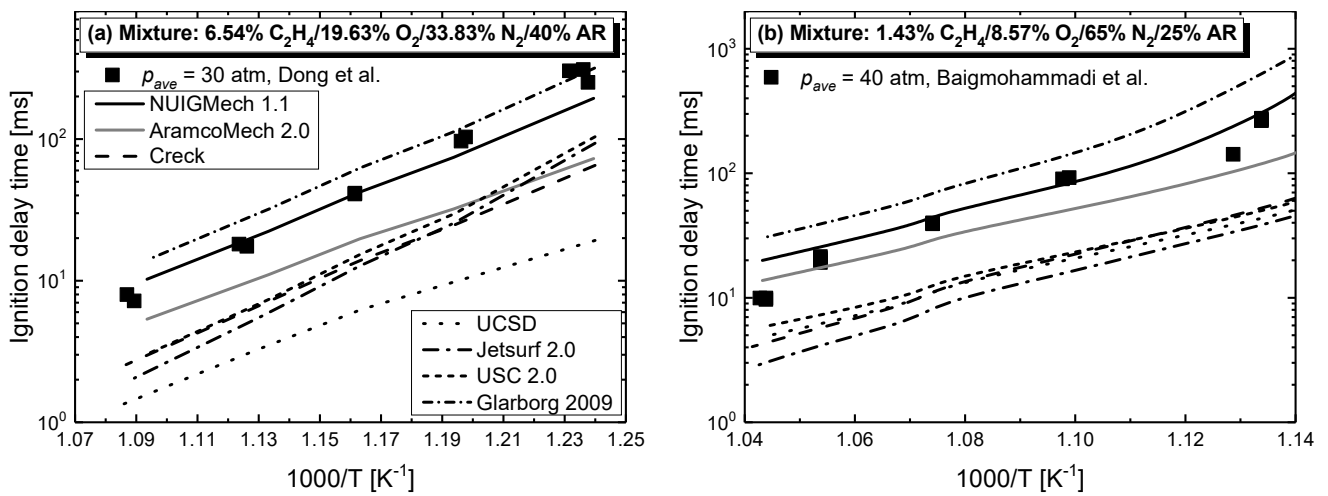
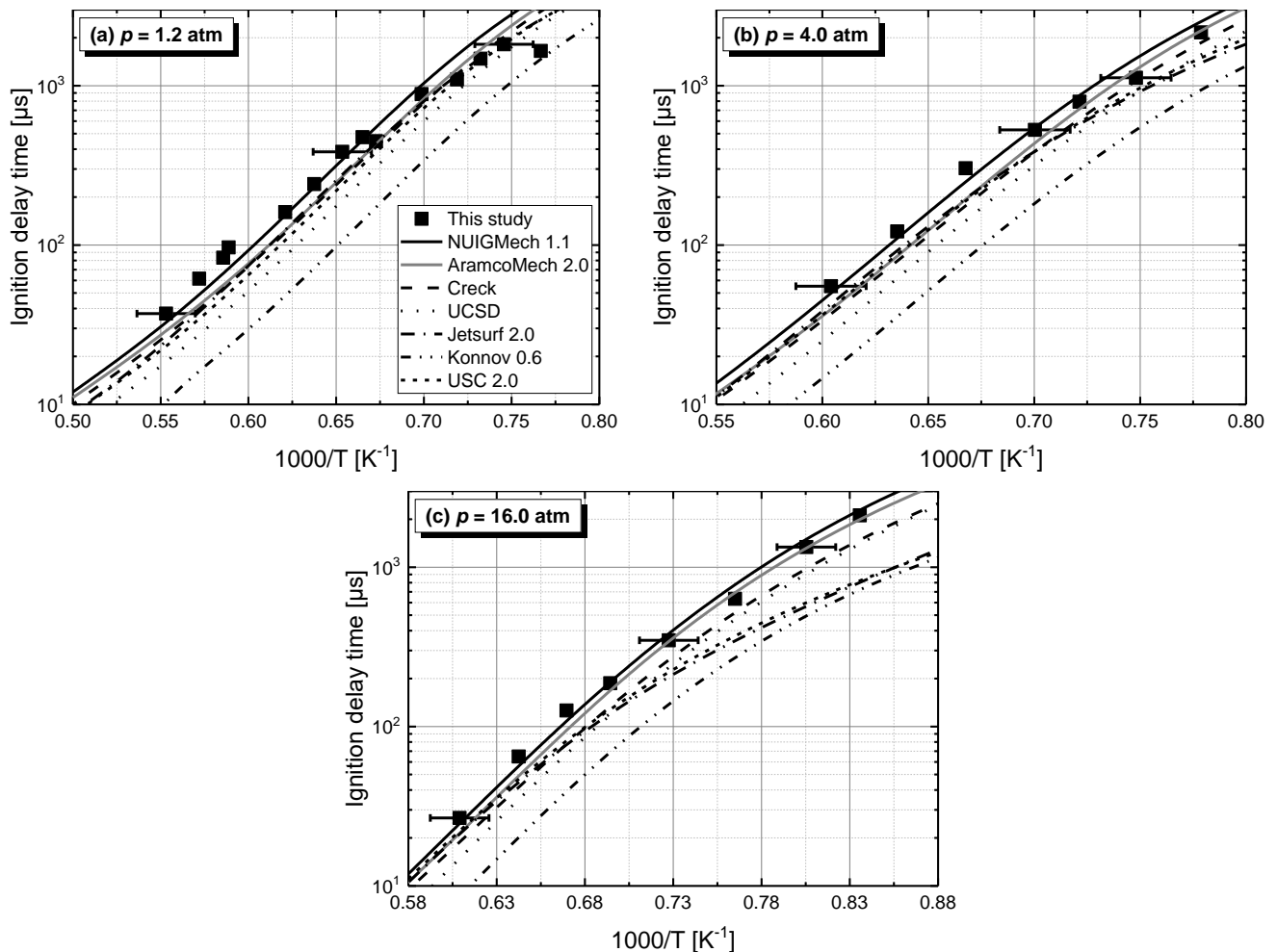


Figure 5. Comparison of measured and simulated IDTs of ethylene with shock tube at 1.2 atm (a), 4.0 atm (b) and 16.0 atm (c). Symbols: experiments in this study, lines: model simulations.



**Figure 6.** Comparison of measured and simulated IDTs of ethylene with RCM at 30 atm (a) and 40 atm (b). Symbols: experiments from Dong et al. [29] and Badig Mohammadi et al. [28], lines: model simulations.



**Figure 7.** Comparison of measured and simulated IDTs of propene with shock tube at 1.2 atm (a), 4.0 atm (b) and 16.0 atm (c). Symbols: experiments in this study, lines: model simulations.

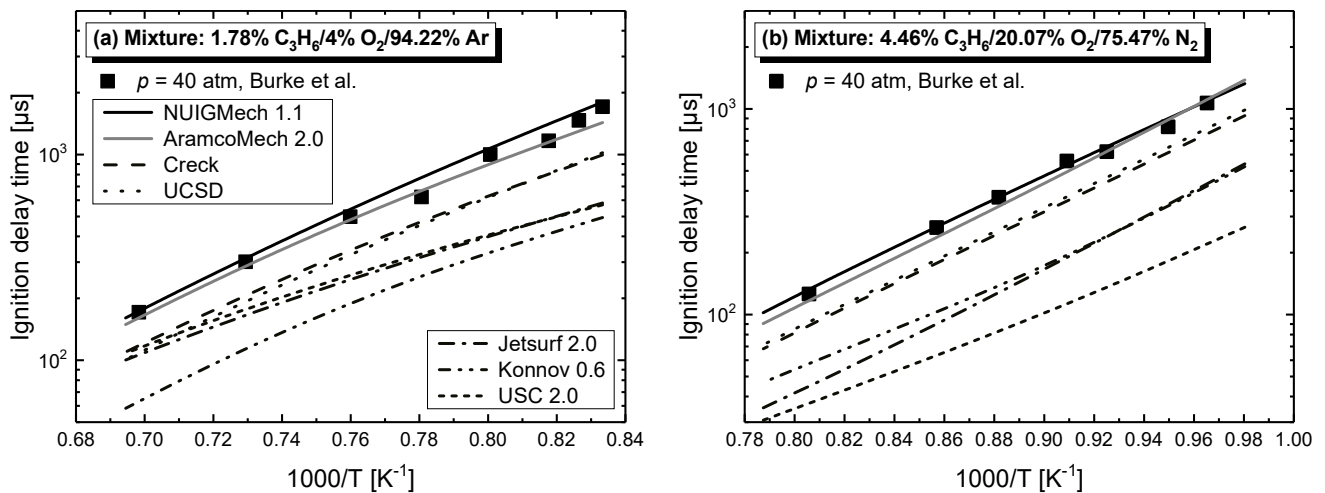


**Figure 8.** Comparison of measured and simulated IDTs of propene with RCM for fuel in argon mixture (a) and fuel in air mixture (b). Symbols: experiments from Burke [39], lines: model simulations.

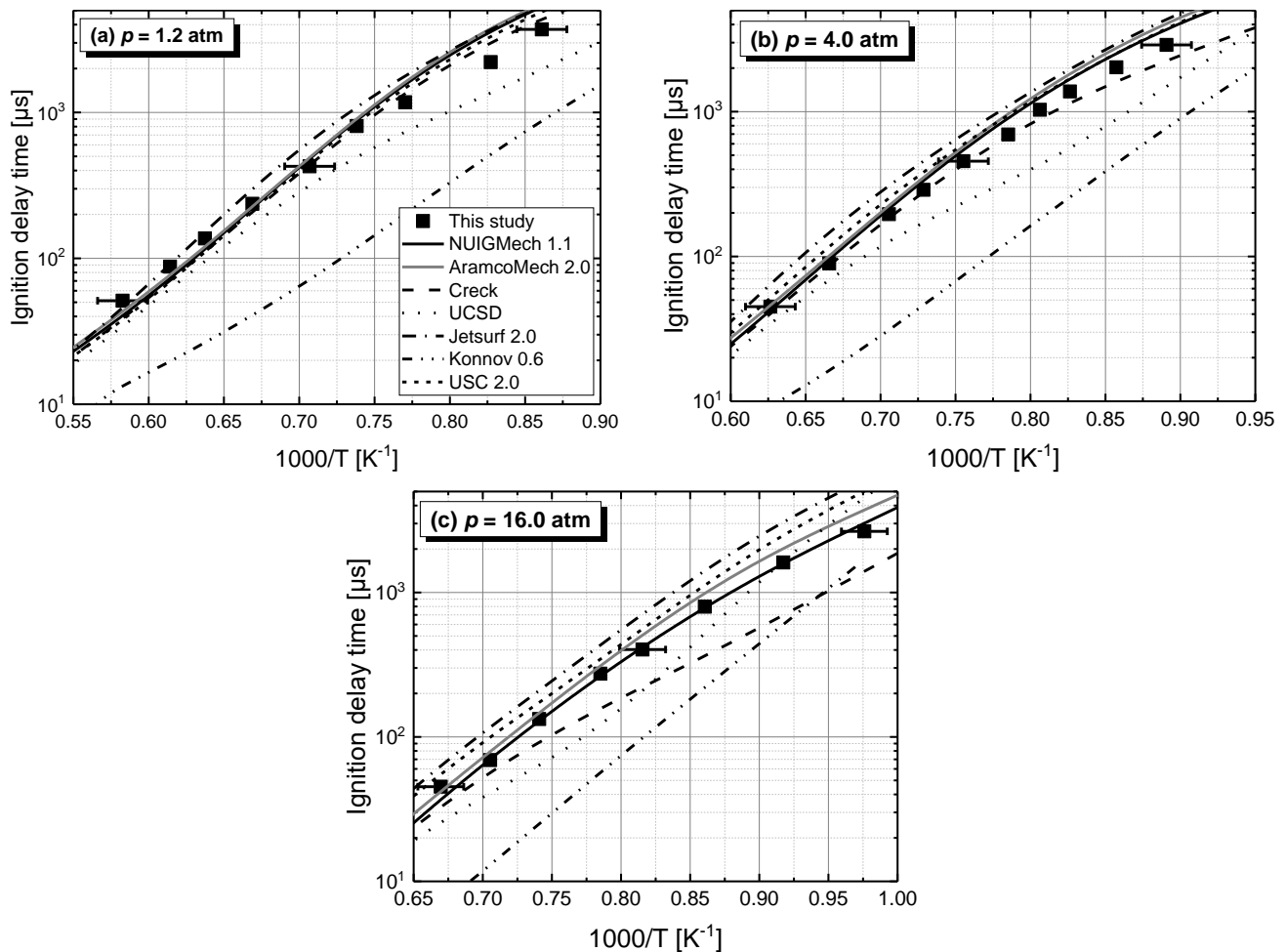


**Figure 9.** Comparison of measured and simulated IDTs of 1-butene with shock tube at 1.2 atm (a), 4.0 atm (b) and 16.0 atm (c). Symbols: experiments in this study, lines: model simulations.

For ethylene, all the selected models, NUIGMech 1.1, AramcoMech 2.0, UCSD and ChuanDa all predict measured IDTs well at all pressures, (Figure 5). Both Creck and Jetsurf 2.0 agree fairly well at 1.2 atm, while they show poor performance at high pressures,

which are both approximately two times slower compared to the present data at 16.0 atm. Konnov 0.6 yields lower reactivity especially at lower pressures, which is about two times longer compared with experimental data at 1.2 atm. USC 2.0 produces approximately 2.5 times slower IDTs compared to the present data at both 1.2 and 4.0 atm, while it agrees fairly well at 16.0 atm. On the contrary, Glarborg 2009 predicts well at both 1.2 atm and 4.0 atm, while it exhibits approximately two times faster than present data. Regarding the experimental data obtained by RCM in Figure 6, Only NUIGMech 1.1 performs great predictions. Glarborg 2009 gives slightly longer IDTs, while other models predict lower IDTs, indicating that the low-temperature chemistry of these modes is still flawed. It is worth noting that the Konnov 0.6 model does not converge when calculating RCM experimental results. Besides, the temperature and pressure at the end of the compression pressure calculated by ChuanDa model using the volume history are far larger than the experimental results.

For propene, both NUIGMech 1.1 and AramcoMech 2.0 predict fairly well the IDT at all three pressures, (Figure 7). Creck, Jetsurf 2.0 and USC 2.0 give acceptable agreement at 1.2 and 4.0 atm at whole temperatures, but show different levels of under-prediction at 16.0 atm and lower temperature. Besides, UCSD exhibits mildly higher reactivity at all present studied conditions. However, Konnov 0.6 yields approximately 3.5 times lower values compared to present data for all of three pressures. As for the data obtained by RCM in Figure 8, again, both NUIGMech 1.1 and AramcoMech 2.0 predict fairly well the data, while all other models show poor performance and underestimate IDTs.

For 1-butene, both NUIGMech 1.1 and AramcoMech 2.0 still predict fairly well the measured data at all pressures, (Figure 9). The Creck model shows good performance at both 1.2 and 4.0 atm, while it under-predicted experimental data at 16.0 atm and lower temperature. UCSD can only capture IDTs at higher temperature regions of both 1.2 atm and 4.0 atm. Jetsurf 2.0 and USC 2.0 give acceptable agreement at 1.2 and 4.0 atm at whole temperatures, but show different levels of over-prediction at 16.0 atm. However, Konnov 0.6 yields approximately five times lower values compared to present data for all three pressures. For the data obtained by RCM (Figure 10), NUIGMech 1.1 and AramcoMech 2.0 predict fairly well the data, while all other models show poor performance and underestimate the IDTs

Through the comparison above, the NUIGMech 1.1 mechanisms show better performance in terms of predicting IDTs of C<sub>2</sub>–C<sub>4</sub> 1-alkenes over all the test conditions. Thus, this mechanism is selected to perform the following chemical kinetic analysis.

## 4.2. Auto-Ignition of C<sub>2</sub>–C<sub>4</sub> 1-Alkenes

### 4.2.1. Pressure Dependent Behavior

Figure 11 presents the IDTs of ethylene at pressures varying from 1.1 atm to 17.9 atm. It generally exhibits a promoting effect of pressure on reactivity. However, this pressure dependence tends to be inapparent with decreasing temperature, and it certainly converges to a point where it shows pressure independence. To clear this tendency, the NUIGMech 1.1 was adopted to simulate the IDTs of ethylene mixtures at pressures of 1–64 atm with temperatures of 720–2240 K, (Figure 11(b<sub>2</sub>)). It is similar to the experimental observation, different pressure dependences of ethylene IDTs, promoting effects at both high- and low-temperatures, while independence at intermediate temperatures can be observed. This non-linear pressure dependence is mainly caused by competition between chain branching and chain termination in the H/O<sub>2</sub> system. At lower temperatures, fuel is consumed via H-abstraction reactions by OH radicals and O atoms, followed by reaction of vinylic radicals and O<sub>2</sub> molecules. With increasing pressure, rate constants of these reactions will be increased due to increased concentration. Thus, IDTs show clear pressure dependences at lower temperatures. At intermediate to high temperatures, the chain branching reaction  $\dot{H} + O_2 \rightleftharpoons \dot{O} + OH$  dominates the system reactivity. At the intermediate temperature and low pressure, O atoms produced by this chain process react with vinylic radicals, reproducing a H atom and a vinylic radical, and in general accelerate ethylene consumption. However,

the chain propagation reaction  $\dot{H} + O_2 (+M) \rightleftharpoons H\dot{O}_2 (+M)$  is intensified with increasing pressure while flux to  $\dot{C}_2H_3 + \dot{O}$  is decreased due to fewer  $\dot{O}$  atom produced by  $\dot{H} + O_2$ , which leads to a more pronounced decrease of the reactivity at intermediate temperatures. It accordingly shows less pressure dependence of IDTs with intermediate temperature. However, at high temperatures, the increase in temperature enables  $\dot{H} + O_2$  to compete for the termination reaction even at higher pressures. Consequently, IDTs show obvious pressure dependence due to the higher reactivity resulting from a concentration effect.

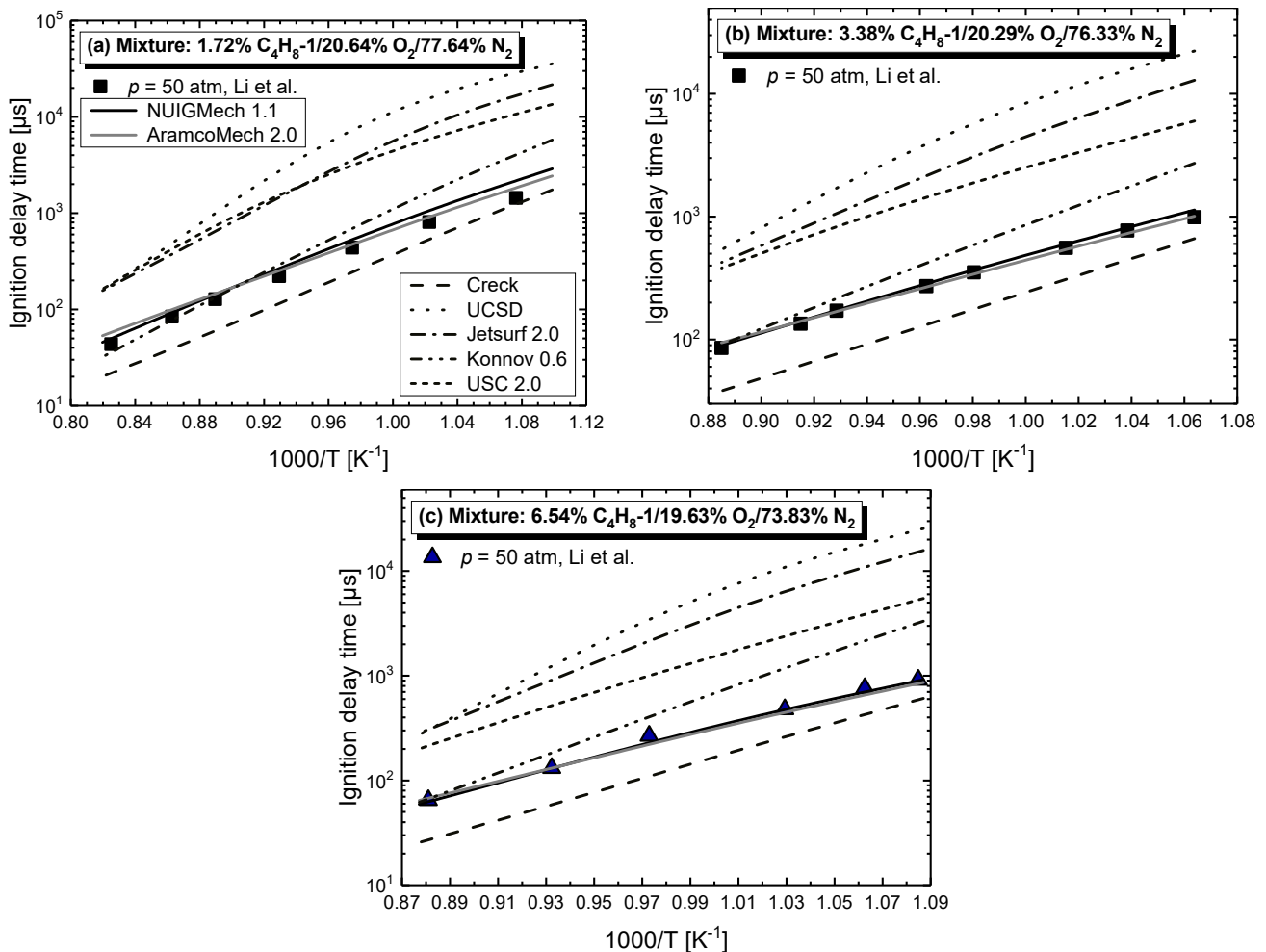


**Figure 10.** Comparison of measured and simulated IDTs of propene with RCM at  $f = 0.5$  (a),  $f = 1.0$  (b) and  $f = 2.0$  (c). Symbols: experiments from Li et al. [43], lines: model simulations.

For propene and 1-butene, however, they also exhibit significant pressure dependence, but without negative pressure effects even at low temperatures, (Figure 12). In addition, the positive pressure dependence appears more obvious at lower temperatures than at high temperatures. It is well known that at high temperatures the pressure-independent  $\dot{H} + O_2 \rightleftharpoons \dot{O} + \dot{O}H$  reaction is the most promoting reaction at both high and low pressures. Parallel to ethylene, the pressure dependence at high temperature is totally caused by the increased concentration with increasing pressure. At lower temperatures, however, the chain branching is no longer dominant and shifts to the collision stabilized pathway  $\dot{H} + O_2 (+M) \rightleftharpoons H\dot{O}_2 (+M)$ , which is a well-known pressure-dependent reaction. Regarding propene, hydroperoxyl radicals can promote fuel oxidation via reacting with stable allyl radicals forming allyl-hydroperoxide radicals, allyl-oxo and hydroxyl radicals. All the reactions mentioned above are geared to be pressure-dependent. Therefore, the rise in reactant concentration is paralleled by the increases of series reactions involving  $H\dot{O}_2$ ,

and both accelerate collectively fuel reactivity and shorten the propene IDTs at lower temperatures. Likewise, main oxidation pathways of 1-butene at lower temperatures are also mostly related to pressure-dependent reactions. For instance, the addition reaction of  $\dot{\text{O}}\text{H}$  to 1-butene reaction and the subsequent addition reaction to oxygen molecules and the formed allylic radicals will undergo the reaction sequence mentioned in low-temperature oxidation of propene.

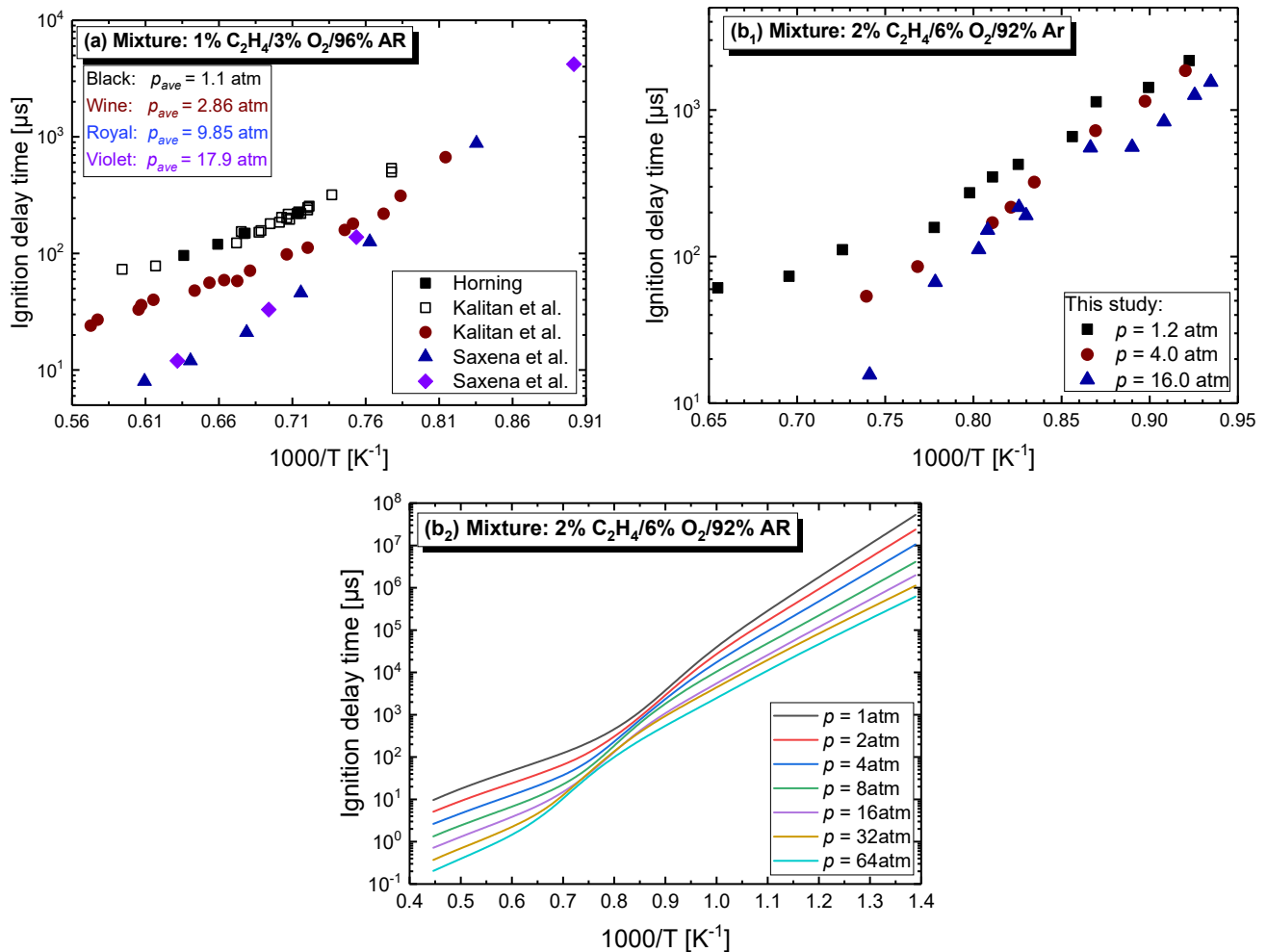


**Figure 11.** Non-linear pressure dependence of ethylene IDTs. (a) data from Horning [15], Kalitan et al. [17], Saxena et al. [21]; (b1) data from this study; (b2) simulations with NUIGMech 1.1.

#### 4.2.2. Equivalence Ratio Dependence

The changing equivalence ratio largely alters concentrations of fuel and oxidizer. We know that reactivity of alkenes is sensitive to reaction  $\dot{\text{H}} + \text{O}_2 \rightleftharpoons \dot{\text{O}} + \dot{\text{O}}\text{H}$  at high temperatures and to fuel concentrations via reactions involving fuel radicals chemistry at low temperature, respectively. For the case of  $\dot{\text{H}} + \text{O}_2 \rightleftharpoons \dot{\text{O}} + \dot{\text{O}}\text{H}$  dominating reactivity, Figure 13(a), an inhibiting effect of equivalence ratio on ethylene IDTs is observed at tested conditions. The  $\text{O}_2$  concentration increased clearly with a decreasing equivalence ratio; accelerating the reaction of  $\dot{\text{H}} + \text{O}_2 \rightleftharpoons \dot{\text{O}} + \dot{\text{O}}\text{H}$  therefore promotes fuel reactivity at high temperatures. However, for the case of fuel radicals dominating reactivity, Figure 13(b<sub>1</sub>), the various equivalence ratio is largely embodied in fuel concentrations changed in the mixtures, at  $T < 1150$  K, a promoting effect of equivalence ratios on ethylene IDTs is exhibited at tested conditions. To make clear the fuel radicals chemistry effect, the NUIGMech 1.1 was adopted to simulate the IDTs of ethylene mixtures at equivalence ratio of 0.5–2.0 with temperatures of 720–1250 K, (Figure 13(b<sub>2</sub>)). The fuel concentration increased clearly

with an increasing equivalence ratio, which accelerates the fuel radicals concentration and therefore promotes fuel reactivity at low temperatures.

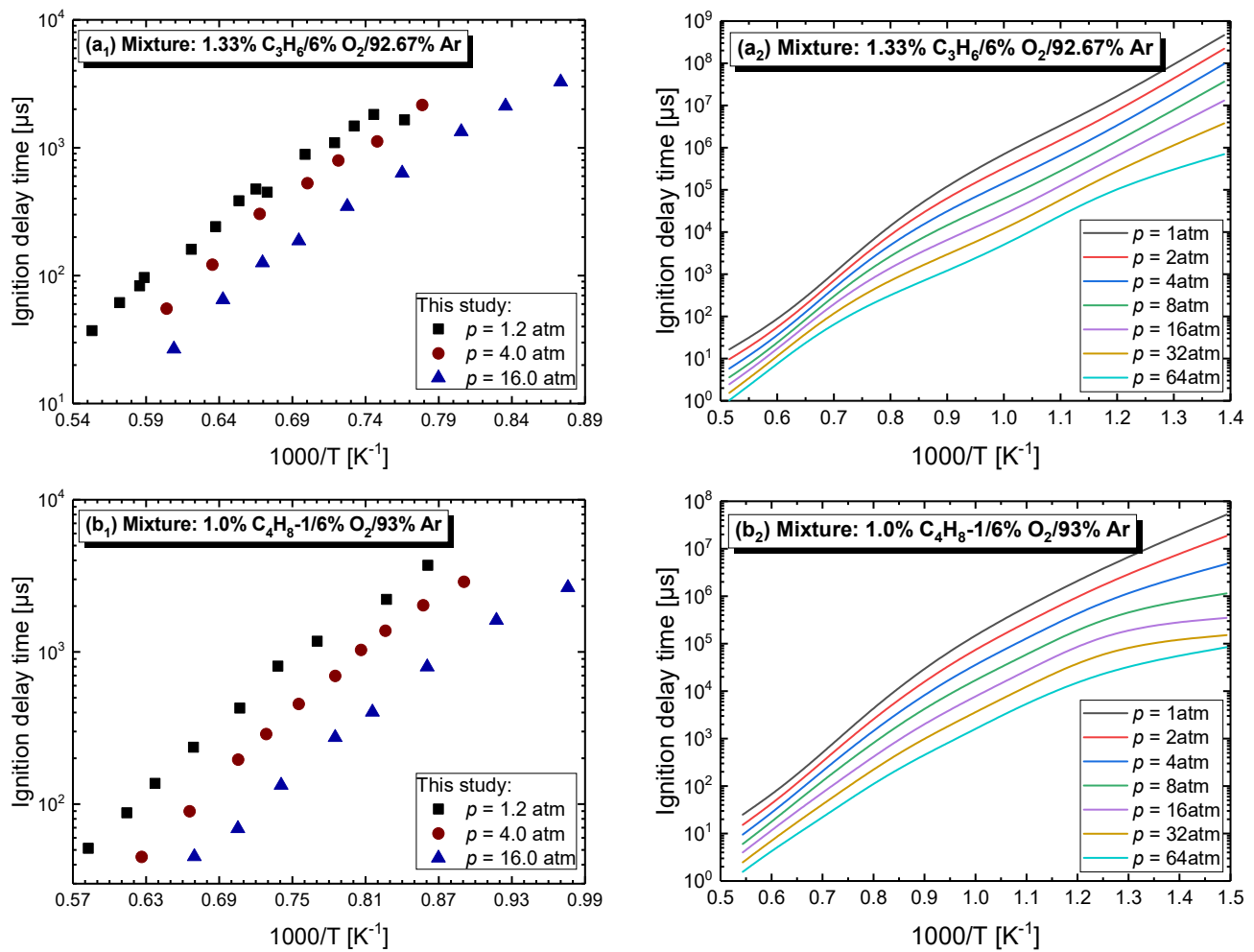


**Figure 12.** Quasi-linear pressure dependence of IDTs of propene and 1-butene. (a<sub>1</sub>)/(a<sub>2</sub>) propene; (b<sub>1</sub>)/(b<sub>2</sub>) 1-butene. Symbols are experimental IDTs from this study; lines are results simulated by NUIGMech 1.1.

For propene and 1-butene, again, the effect of equivalence ratio dependence follows the same rules with ethylene. For the case of reactivity sensitizing reactions  $\dot{H} + O_2 \rightleftharpoons \dot{O} + OH$  at high temperatures, (Figure 14(a<sub>1</sub>,b<sub>1</sub>)), increasing the equivalence ratio inhibits reactivity. Additionally, for the case of reactivity sensitizing fuel radical chemistry at low temperatures, (Figure 14(a<sub>2</sub>,b<sub>2</sub>)), increasing the equivalence ratio promotes reactivity.

#### 4.2.3. Effect of Dilution

Diluted gases do not participate in reaction directly, but they can participate in fuel oxidation indirectly by acting as a third body, which will influence the chemical effective collision coefficient between reactants. Argon can improve the quality of the flow field in the shock tube, reduce the boundary layer thickness caused by the incident shock wave, and lighten the interaction between the reflected shock wave and the boundary layer. At the same time, the characteristic time of reaching thermodynamic equilibrium is shorter due to its single molecular structure; the auto-ignition experimental data is more suitable for validating the chemical kinetic model when the argon gas is diluted. Nitrogen as diluted gas is closer to the combustion in the actual combustion device. Thus, argon and nitrogen are always selected as diluted gases.

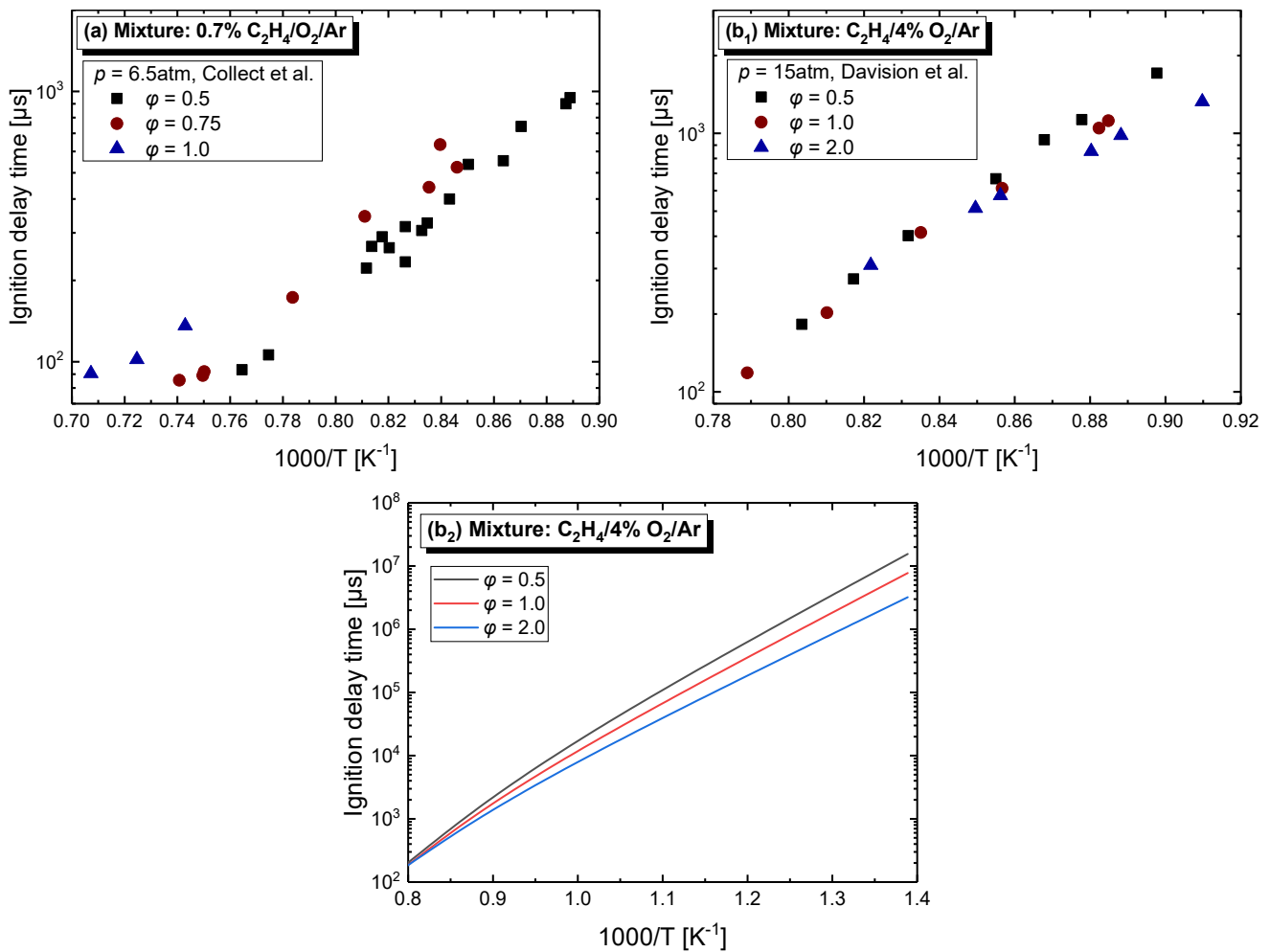


**Figure 13.** Equivalence ratio dependence of ethylene IDTs. (a) case of  $\dot{H} + O_2 \rightleftharpoons \ddot{O} + \dot{OH}$  dominating reactivity at high temperature; (b<sub>1</sub>)/(b<sub>2</sub>) case of fuel radicals dominating reactivity at low temperature; lines are results simulated by NUIGMech 1.1.

Figure 15 shows constant volume adiabatic simulations of the effect of dilution from 75% to 95% on IDTs for ethylene, propene and 1-butene at equivalence ratios of 1.0 and pressures of 10.0 atm using NUIGMech 1.1. As expected, increasing dilution results in a decrease in reactivity for all three alkenes. At 1000 K, for ethylene, increasing dilution to 85% and 95% can increase IDT to about 61.6% and 3.1 times, respectively. For propene, IDT increased approximately 1.3 and 17.8 times when dilution increased to 85% and 95%, respectively. Additionally, regarding 1-butene, it was around 69.5% and 5.54 times enlarged with adding dilution from 75% to 85% and 95%, respectively. It shows that the reactivity of propene's mixtures is more sensitive to dilution. Besides, the dilution ratio also has a great influence on the auto-ignition mode of the fuel. At higher dilution mixtures, weak ignition is prone to occur. Specifically, the pressure rise is unobvious when ignition occurs. However, strong ignition is expected in the mixtures with a lower dilution ratio. Combustion occurs instantaneously with a large amount of heat release associated with such mixtures. The combustion wave is generated to compress the unburned gas, which the detonation will be developed more easily. Strong ignition can be distinguished by observing the sharp spikes in the pressure profiles.

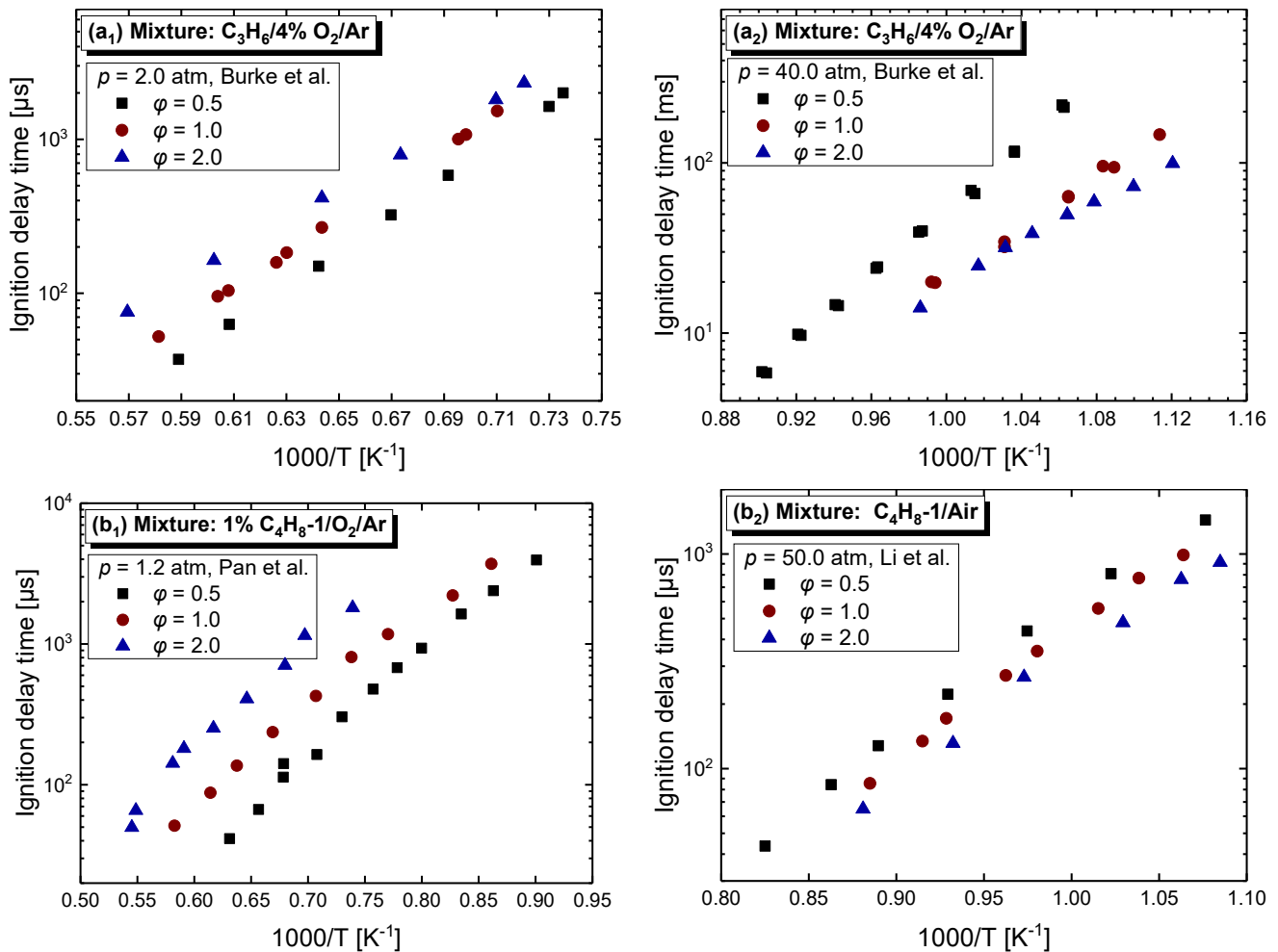


**Figure 14.** Equivalence ratio dependence for IDTs of propene and 1-butene. (a<sub>1</sub>)/(a<sub>2</sub>) Propene, symbols are experimental IDTs from Burke et al. [39]; (b<sub>1</sub>)/(b<sub>2</sub>) 1-butene, symbols are experimental IDTs from Pan et al. [42] and Li et al. [43].

#### 4.3. Arrhenius-Type Correlation of C<sub>2</sub>–C<sub>4</sub> 1-Alkenes

Ignition delay time is a fundamental parameter, not only as a reaction mechanism validation but also as combustor design. A simple relation of IDTs is actually more favorable for engineering applications, and it pushes researchers to make an accurate fitting relationship of IDTs. A modified Arrhenius-type correlation is most commonly used for doing this,

$$\tau_{ign} = A \cdot p^a \phi^b X_{O_2}^c \exp \frac{E_a}{RT} \quad (1)$$

where  $\tau_{ign}$  is the IDT in  $\mu\text{s}$ ,  $A$  is the empirically determined constant,  $p$  is the pressure in atm,  $T$  is the temperature in K and  $X_{O_2}$  is the mole fraction of oxygen molecular,  $E_a$  is the global activation energy in kcal/mol, and  $R$  is the universal gas constant. To consider the effect of dilution, we have introduced new terms including concentrations of argon and nitrogen,

$$\tau_{ign} = A \cdot p^a T^b X_{O_2}^c [1 - X_{Ar}]^d [1 - X_{N_2}]^e \exp \frac{E_0}{RT} \quad (2)$$

where the item of  $X_{O_2}^c [1 - X_{Ar}]^d [1 - X_{N_2}]^e$  is used to describe the mixtures diluted by different inert gases (Ar, N<sub>2</sub> and Ar/N<sub>2</sub> mixtures).

From Equation (1), we obtain a total derivative relation:

$$\frac{d \ln(\tau_{ign})}{dT} = - \frac{E_a}{RT^2} \quad (3)$$

Likewise, from Equation (2), it can be deduced as follows:

$$\frac{d \ln(\tau_{ign})}{dT} = \frac{b}{T} - \frac{E_0}{RT^2} \quad (4)$$

The  $E_a$  in Equation (2) is thus equal to  $E_0 - bRT$ .

With the data collection, three correlations and their relevant parameters are derived individually for ethylene, propene and 1-butene mixtures over a wide range of pressures, temperatures, equivalence ratios and dilutions (Table 4). To avoid non-ideal effects on the ST data and heat release effect on the RCM data, we have pre-processed the experimental data before fitting the correlation. Specifically, for ethylene, the RCM data from Baigmohammadi et al. [28] were replaced by the results simulated by NUIGMech 1.1 with the constant volume approach. The data from Yang et al. [32] can be predicted only by their model, thus the IDTs data over 1000  $\mu\text{s}$  were replaced by the results simulated by the ChuanDa model, also with the constant volume approach. For both propene and 1-butene, NUIGMech 1.1 was used to address the collected data in the same way.

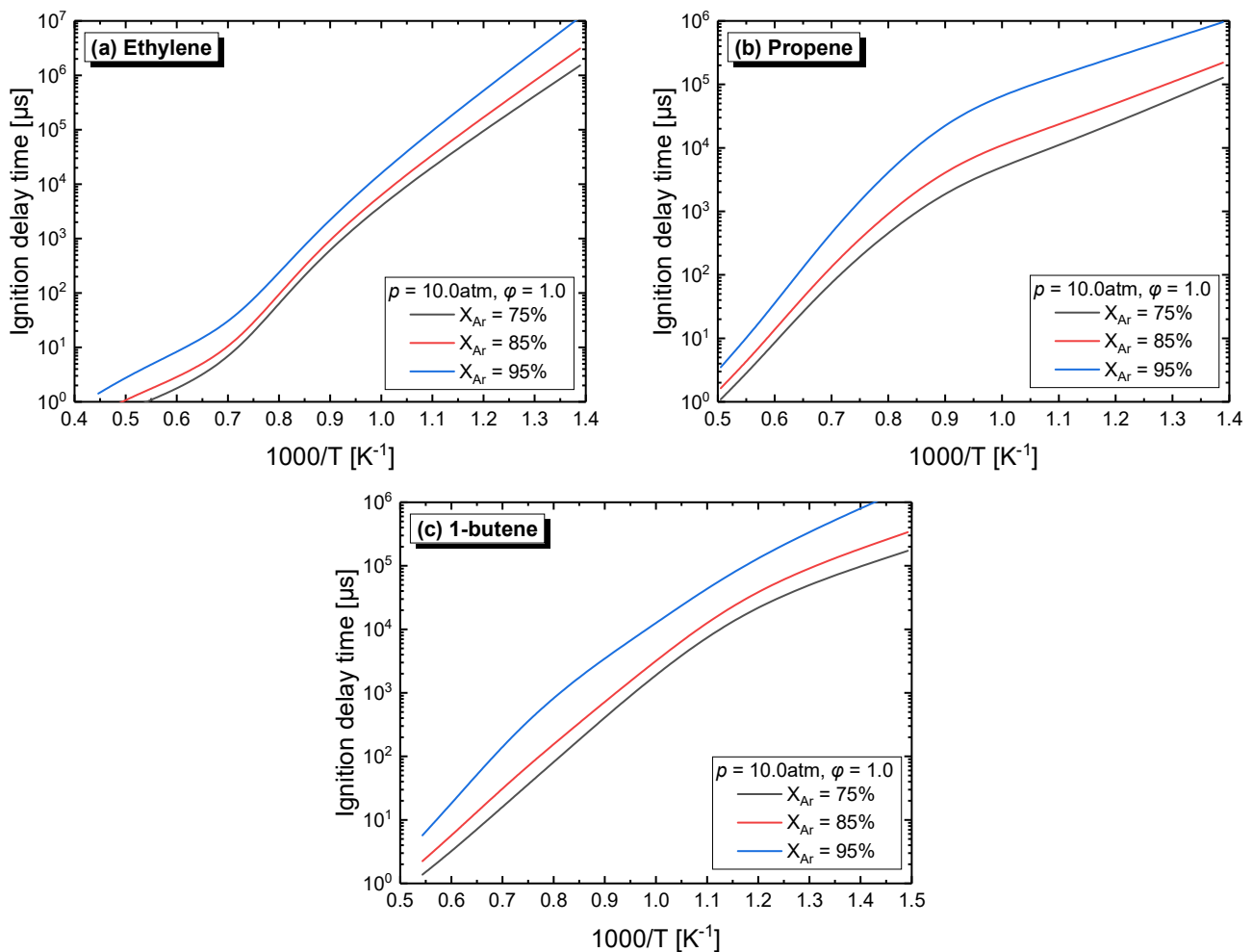


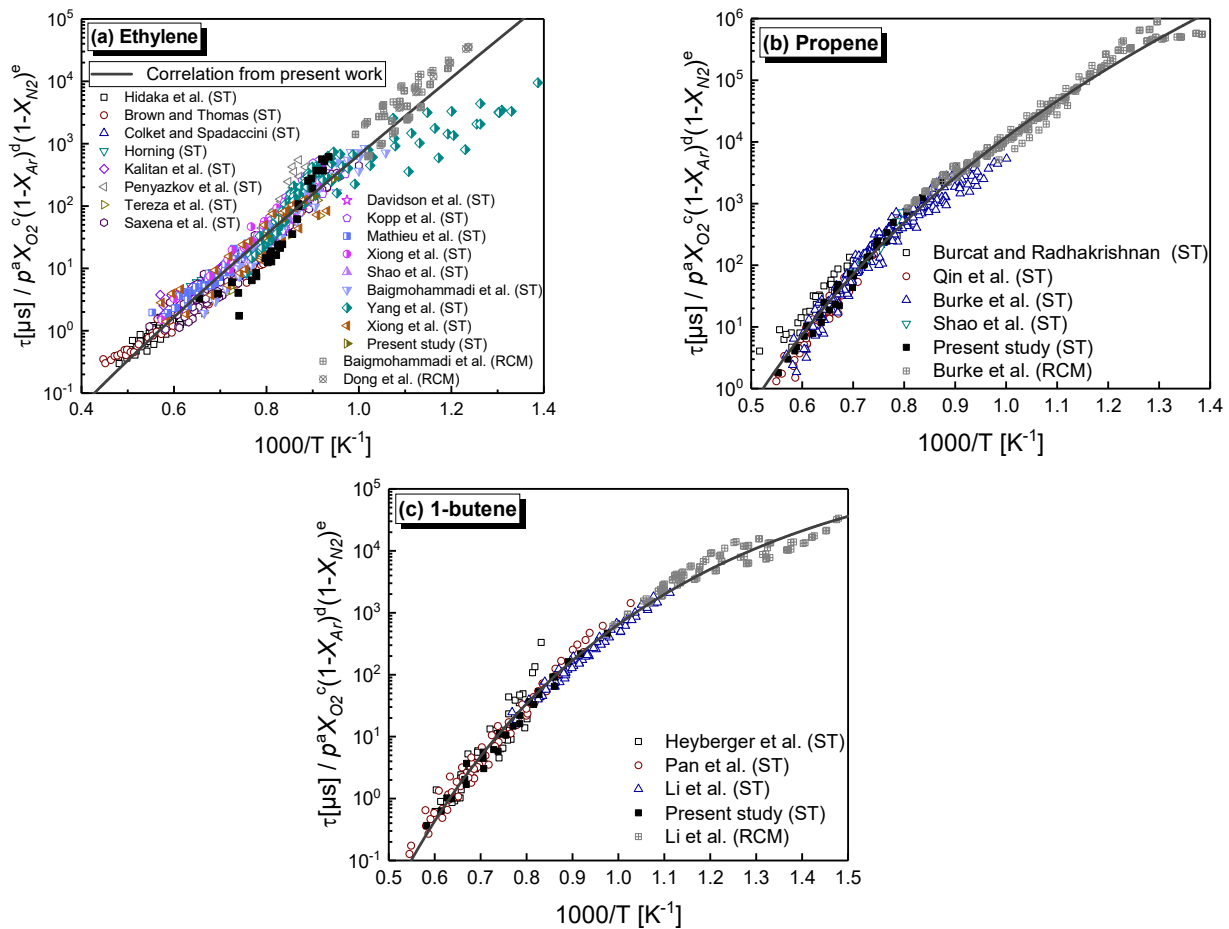
**Figure 15.** Constant volume adiabatic simulation of effect of dilution on IDTs for ethylene, propene and 1-butene using NUIGMech 1.1. (a) Ethylene; (b) propene; (c) 1-butene.

As shown in Figure 16, all data from the present study and literature studies could be fit into this single form correlation. However, for ethylene, IDTs from Yang et al. [32] at a low-temperature range (700–1000 K) diverged from the results of the global fitting, which were lower than other data. Thus, more ST experimental studies are needed to verify IDTs characteristics under such conditions.

**Table 4.** Evaluated coefficients of Arrhenius correlation for C<sub>2</sub>–C<sub>4</sub> 1-alkenes.

Fuel	Data Points	<i>A</i>	<i>a</i>	<i>b</i>	<i>c</i>	<i>d</i>	<i>e</i>	<i>E</i> <sub>0</sub>	<i>R</i> <sup>2</sup>
Ethylene	1039	1.79 × 10 <sup>3</sup>	−0.28 ±0.02	−1.94 ±0.68	−1.38 ±0.07	0.58 ±0.07	0.53 ±0.07	24.76 ±1.69	0.92
Propene	595	4.02 × 10 <sup>50</sup>	−0.80 ±0.02	−15.34 ±0.66	−1.19 ±0.04	0.07 ±0.04	0.12 ±0.05	−2.29 ±1.41	0.98
1-Butene	315	1.16 × 10 <sup>73</sup>	−0.94 ±0.02	−22.00 ±0.66	0.57 ±0.04	−2.53 ±0.04	−3.12 ±0.05	−19.48 ±1.6	0.97

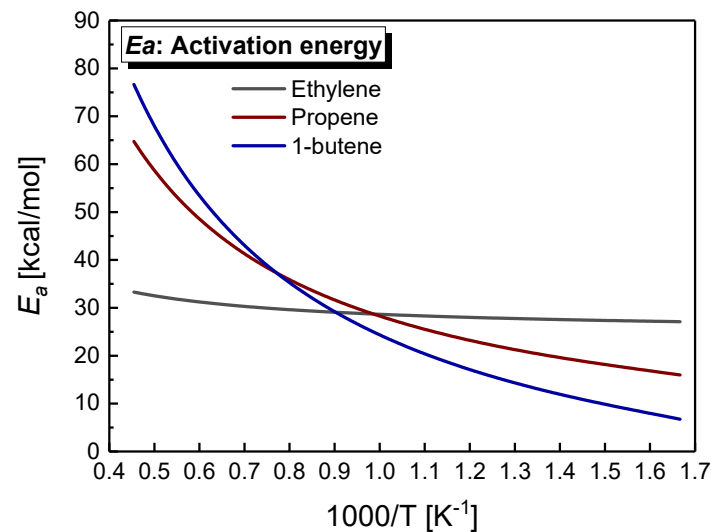
Black: original value; blue: standard error.



**Figure 16.** Arrhenius-type correlations of IDTs for ethylene (a), propene (b) and 1-butene (c). Symbols: experimental data from literatures (Hidaka et al. [13], Brown and Tomas [14], Colket and Spadaccini [16], Horning [15], Kalitan et al. [17], Penyazkov et al. [19], Tereza et al. [20], Saxena et al. [21], Davidson et al. [22], Kopp et al. [23,24], Mathieu et al. [25], Xiong et al. [26], Shao et al. [27], Baigmohammadi et al. [28], Yang et al. [32], Xiong et al. [31], Dong et al. [29], Burcat and Radhakrishnan [34], Qin et al. [35], Burke et al. [38,39], Heyberger et al. [36], Pan et al. [42], Li et al. [43]) and present study, lines: correlation predictions.

Figure 17 shows comparisons of global activation energy for ethylene, propene and 1-butene with temperatures of 600–2200 K. The  $E_a$  of 1-butene and propene show similar temperature dependence and generally decreases with decreasing temperature. It means the dominant reaction kinetics of auto-ignition change greatly from high to low temperature. The  $E_a$  of ethylene, however, does not make significant changes with temperature increasing, indicating that a similar reaction mechanism dominates the ignition kinetics at both high and low temperatures. The  $E_a$  shows in order of 1-butene, propene and ethylene at the high-temperature side (>1300 K), where ethylene has the highest reactivity and is

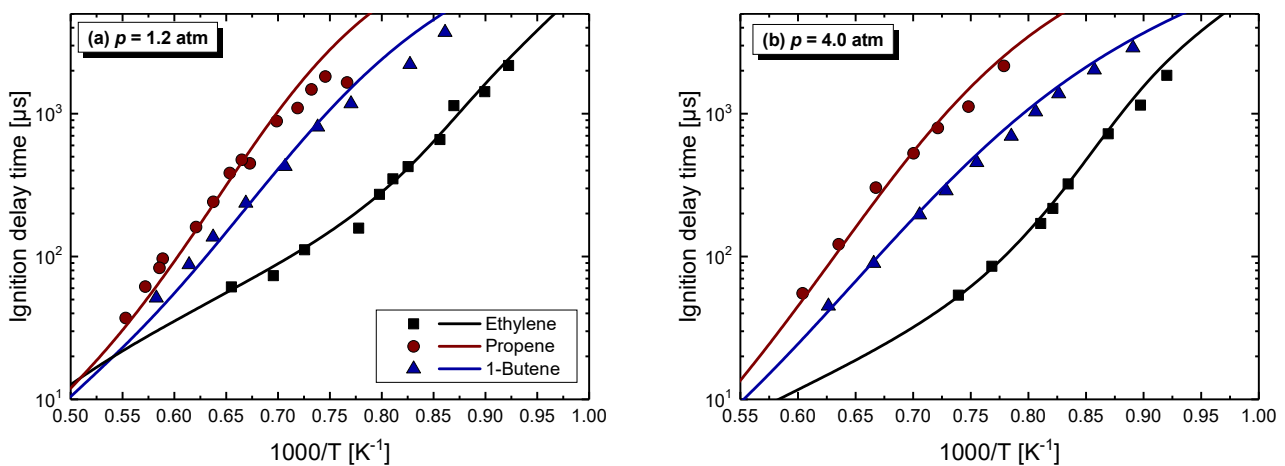
easy to ignite. With the temperature going down, the 1-butene had the lowest activation energy and is most likely to ignite.



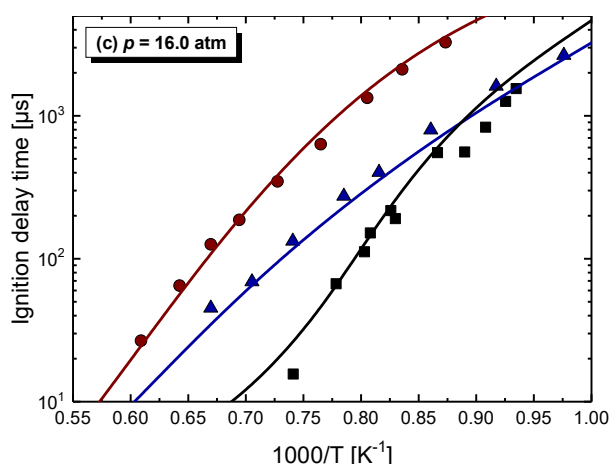
**Figure 17.** Comparison of global activation energy for ethylene, propene and 1-butene predicted by  $E_a$  deduced from Equation (2).

### 5. Reactivity Comparison at High Temperature

Ignition delay time is a global parameter to represent the reactivity of fuel, which is primarily governed by fuel kinetics. Figure 18 gives the reactivity comparison for stoichiometric ethylene, propene and 1-butene together, with the calculated results using NUIGMech 1.1 at pressures of 1.2, 4.0 and 16.0 atm over temperatures of 1030–1820 K. It can be clearly seen that ethylene shows the highest reactivity, propene gives the lowest ones, while 1-butene lies in-between. More specifically, at a lower pressure (1.2 atm), these three alkenes show similar reactivity when the  $T > 1700$  K, while the reactivity order accords with the above law when the  $1200 \text{ K} < T < 1700$  K. With the pressure increased, the order of reactivity for these alkenes was consistent with the above law within all the studied temperature ranges. It was mentioned that the reactivity intensity of ethylene was decreased with the pressure increase. For example, at 1250 K, the IDT of propene and 1-butene was about 19.7 and 6.3 times than that of ethylene, respectively, at 1.2 atm, but only about 9.8 and 3.2 times, respectively, at 16.0 atm.



**Figure 18.** Cont.



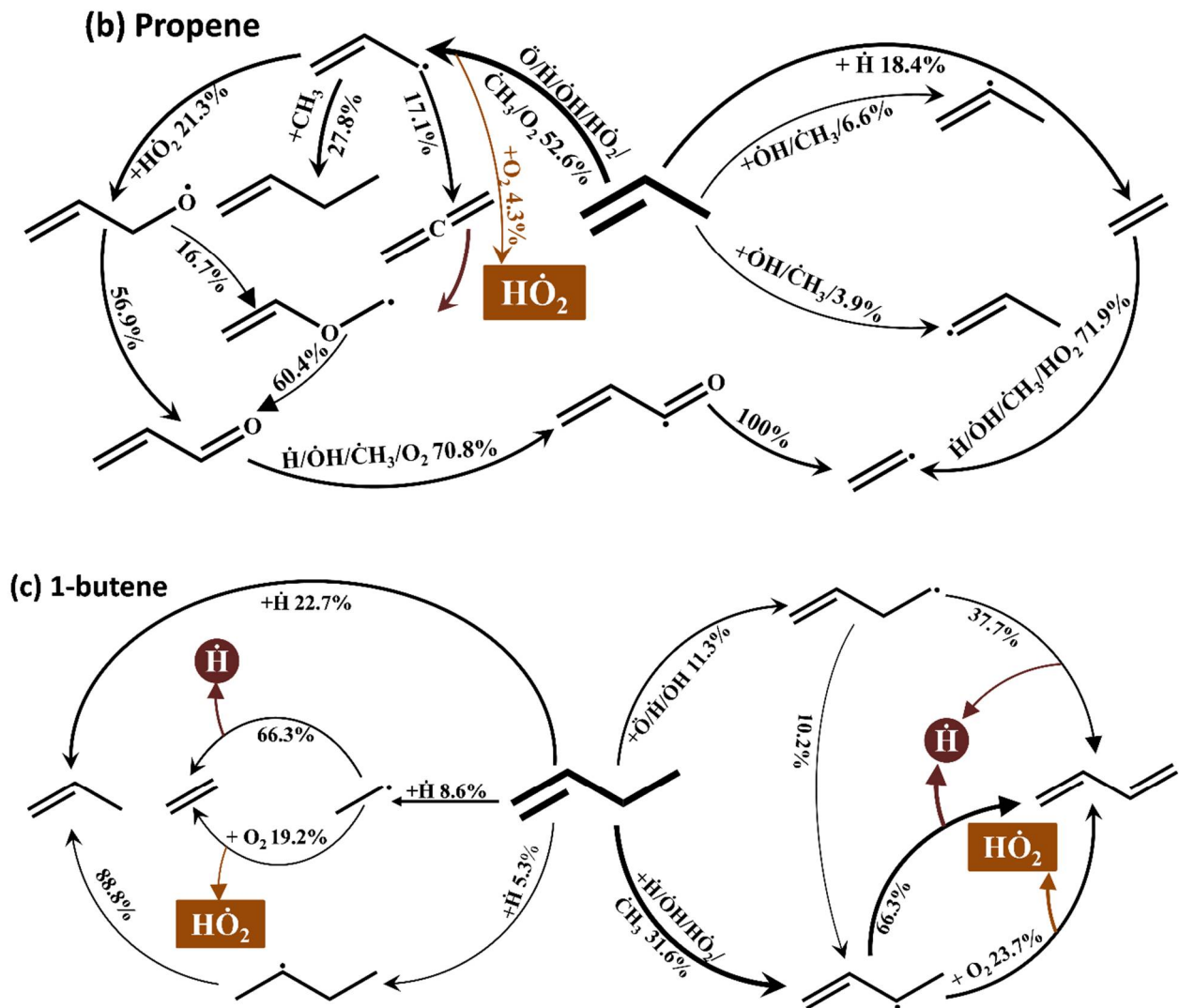
**Figure 18.** Reactivity comparisons of C<sub>2</sub>–C<sub>4</sub> 1-alkanes at 1.2 atm (a), 4.0 atm (b) and 16.0 atm (c). Symbols denote experimental data measured in this study. Lines denote model simulations with NUIGMech 1.1.

Figure 19 depicts brute force sensitivity coefficients of IDT to the rate constants for ethylene, propene and 1-butene oxidation at 1250 K and 16 atm. Regarding ethylene, reactivity shows notably larger sensitivity to the chain branching reaction ( $\dot{\text{H}} + \text{O}_2 \rightleftharpoons \ddot{\text{O}} + \dot{\text{O}}\text{H}$ ), as shown in Figure 19a. Reaction flux analysis at the same conditions shows that almost 46.8% ethylene is consumed by H-abs producing vinyl radicals, Figure 20a. Subsequently, 34.4% of vinyl radicals are consumed by the major chain branching reaction pathway of  $\dot{\text{C}}_2\text{H}_3 + \text{O}_2 = \dot{\text{C}}\text{H}_2\text{CHO} + \ddot{\text{O}}$ , followed by  $\dot{\text{C}}\text{H}_2\text{CHO}$  decomposition leading to the formation of  $\dot{\text{H}}$  atoms, which pronouncedly promote reactivity. Moreover, 19.9% of ethylene reacts with  $\ddot{\text{O}}$  atom to form the  $\dot{\text{H}}$  atom. These can further produce  $\ddot{\text{O}}$  atom and  $\dot{\text{O}}\text{H}$  radicals via the most important chain-branching reaction  $\dot{\text{H}} + \text{O}_2 \rightleftharpoons \ddot{\text{O}} + \dot{\text{O}}\text{H}$ . This is the reason why the ethylene presents relatively higher reactivity at high temperatures.

However, for propene, the most reactivity-dominated reaction is  $\text{C}_3\text{H}_6 + \text{O}_2 \rightleftharpoons \dot{\text{C}}_3\text{H}_5\text{-A} + \text{H}\dot{\text{O}}_2$ , meaning  $\text{H}\dot{\text{O}}_2$  radicals are crucial for the oxidation of propene, Figure 19b. As shown in Figure 20b, about 52.6% of propene flux leads to the formation of allylic radicals. Additionally, then, the allylic radical recombines with the  $\dot{\text{C}}\text{H}_3$  radical (27.8%) or is consumed by  $\text{H}\dot{\text{O}}_2$  radicals (21.3%). Between these two pathways, the reaction with  $\text{H}\dot{\text{O}}_2$  radicals is a system reactivity, preferred due to the fact that it ultimately leads to the formation of allyloxy and hydroxyl radicals, which is chain-branching, competing with recombination, which is chain terminating. Unfortunately, there are really few reaction pathways to generate  $\text{H}\dot{\text{O}}_2$  during propene oxidation. As a result, propene shows the longest IDTs among the three alkenes.

For 1-butene, the reaction  $\dot{\text{H}} + \text{O}_2 \rightleftharpoons \ddot{\text{O}} + \dot{\text{O}}\text{H}$  dominates reactivity. The second pathway promoting reactivity is the reaction  $\dot{\text{C}}_4\text{H}_7\text{-1-3} + \text{O}_2 \rightleftharpoons \text{C}_4\text{H}_6 + \text{H}\dot{\text{O}}_2$ , which consumes a stabilized allylic radical to generate a more reactive  $\text{H}\dot{\text{O}}_2$  radical, (Figure 19c). As shown in Figure 20c, About 31.6% of 1-butene are consumed via H-abs, producing allylic  $\dot{\text{C}}_4\text{H}_7\text{-1-3}$  radicals. The  $\dot{\text{C}}_4\text{H}_7\text{-1-3}$  radical is mainly consumed via two pathways. First, it decomposes (66.3%) directly into a 1,3-butadiene molecular and a  $\dot{\text{H}}$  atom, which promotes the reactivity, as it transfers a very stabilized allylic radical to a reactive  $\dot{\text{H}}$  atom that can further undergo a chain branching reaction  $\dot{\text{H}} + \text{O}_2 \rightleftharpoons \ddot{\text{O}} + \dot{\text{O}}\text{H}$ . Second, it reacts (23.7%) with  $\text{O}_2$  to generate 1,3-butadiene and a  $\text{H}\dot{\text{O}}_2$  radical; again, this pathway promotes reactivity as discussed above. About 22.7% of 1-butene reacts with H-atoms to form propene and  $\dot{\text{C}}\text{H}_3$  radicals. Next, the reaction path flows to propene flux, which needs abundant  $\text{H}\dot{\text{O}}_2$  radicals to consume allylic  $\text{C}_3\text{H}_5\text{-A}$  radicals. Unlike propene, the reaction pathway for  $\text{H}\dot{\text{O}}_2$  formation in 1-butene is efficient, mainly including reactions  $\dot{\text{C}}_4\text{H}_7\text{-1-3} + \text{O}_2 \rightleftharpoons \text{C}_4\text{H}_6 + \text{H}\dot{\text{O}}_2$  and  $\dot{\text{C}}_2\text{H}_5 + \text{O}_2 = \text{C}_2\text{H}_4 + \text{H}\dot{\text{O}}_2$ . Thus, 1-butene presents a higher reactivity compared to propene.





**Figure 20.** Reaction fluxes of  $C_2$ – $C_4$  1-alkenes at 1250 K, 16 atm and 20% fuel conversion. (a) Ethylene, (b) propene, (c) 1-butene.

## 6. Concluding Remarks

Combustion and auto-ignition characteristics for three alkenes (ethylene, propene and 1-butene) were performed both experimentally and theoretically. The main results are summarized as follows:

- (1) Chemical kinetics scheme of 1-alkenes was highlighted according to the precious chemical studies on alkenes. Pressure-dependence of ethylene shows much more difference compared with propene and 1-butene due to different oxidation mechanisms at low temperatures. Nine generally accepted mechanisms, developed by different research groups, and published in recent years were used to simulate the ignition delay times from literature and the current study, only NUIGMech 1.1 was capable of representing the chemical reactivity for all of the three alkenes at all tested conditions.
- (2) A new type of Arrhenius correlation for the three alkenes was proposed against all the ignition data measured in the literature and this study, that can capture the various activation energy with temperature for propene and 1-butene due to essential difference chemistry at high and low-temperatures. The correlations can be used to predict IDTs in engineering with a wide range of pressure, temperature, equivalence ratio and dilution.
- (3) At high temperatures, ethylene shows the shortest ignition delay times, while propene shows the longest ones, with intermediate reactivity for 1-butene. The oxidation of

ethylene depends on the H atom, O atom, and OH radical, and the consumption of vinylic radical accelerates the accumulation of the free radical pool, resulting in the highest reactivity of ethylene. The consumption of allylic radicals becomes a decisive step in propene and 1-butene by HO<sub>2</sub> radicals. However, it has the efficient reaction pathways for HO<sub>2</sub> formation in 1-butene ( $\dot{C}_4H_7 + O_2 \rightleftharpoons C_4H_6 + HO_2$  and  $\dot{C}_2H_5 + O_2 = C_2H_4 + HO_2$ ), but is not involved in propene.

**Supplementary Materials:** The following are available online at <https://www.mdpi.com/article/10.3390/en14185797/s1>.

**Author Contributions:** Conceptualization, W.S., Y.Z., Y.L. and Z.H.; methodology, Y.Z.; software, W.S.; validation, W.S., Y.Z., Y.L. and Z.H.; formal analysis, W.S. and Y.Z.; investigation, W.S. and Y.Z.; data curation, W.S. and Y.Z.; writing—original draft preparation, W.S.; writing—review and editing, Y.Z. and Y.L.; visualization, Y.Z.; supervision, Y.Z.; project administration, Y.Z.; funding acquisition, Y.Z. All authors have read and agreed to the published version of the manuscript.

**Funding:** This research was funded by the Basic Science Center Program for Ordered Energy Conversion of the National Natural Science Foundation of China (No. 51888103), the National Science and Technology Major Project (2017-III-0005-0029) and Science and Technology on Plasma Dynamics Laboratory (No. 614220220200103).

**Institutional Review Board Statement:** Not applicable.

**Informed Consent Statement:** Not applicable.

**Data Availability Statement:** Not applicable.

**Conflicts of Interest:** The authors declare no conflict of interest.

## References

1. Cullen, J.M.; Allwood, J.M. The efficient use of energy: Tracing the global flow of energy from fuel to service. *Energy Policy* **2010**, *38*, 75–81. [CrossRef]
2. Omid, M.; Ghojabeige, F.; Delshad, M.; Ahmadi, H. Energy use pattern and benchmarking of selected greenhouses in Iran using data envelopment analysis. *Energy Convers. Manag.* **2011**, *52*, 153–162. [CrossRef]
3. Ranzi, E.; Cavallotti, C.; Cuoci, A.; Frassoldati, A.; Pelucchi, M.; Faravelli, T. New reaction classes in the kinetic modeling of low temperature oxidation of n-alkanes. *Combust. Flame* **2015**, *162*, 1679–1691. [CrossRef]
4. Metcalfe, W.K.; Burke, S.M.; Ahmed, S.S.; Curran, H.J. A Hierarchical and Comparative Kinetic Modeling Study of C<sub>1</sub>–C<sub>2</sub> Hydrocarbon and Oxygenated Fuels. *Int. J. Chem. Kinet.* **2013**, *45*, 638–675. [CrossRef]
5. Healy, D.; Kopp, M.M.; Polley, N.L.; Petersen, E.L.; Bourque, G.; Curran, H.J. Methane/n-Butane Ignition Delay Measurements at High Pressure and Detailed Chemical Kinetic Simulations. *Energy Fuels* **2010**, *24*, 1617–1627. [CrossRef]
6. Burke, U.; Metcalfe, W.K.; Burke, S.M.; Heufer, K.A.; Dagaut, P.; Curran, H.J. A detailed chemical kinetic modeling, ignition delay time and jet-stirred reactor study of methanol oxidation. *Combust. Flame* **2016**, *165*, 125–136. [CrossRef]
7. Mittal, G.; Burke, S.M.; Davies, V.A.; Parajuli, B.; Metcalfe, W.K.; Curran, H.J. Autoignition of ethanol in a rapid compression machine. *Combust. Flame* **2014**, *161*, 1164–1171. [CrossRef]
8. Dooley, S.; Curran, H.J.; Simmie, J.M. Autoignition measurements and a validated kinetic model for the biodiesel surrogate, methyl butanoate. *Combust. Flame* **2008**, *153*, 2–32. [CrossRef]
9. Metcalfe, W.K.; Togbé, C.; Dagaut, P.; Curran, H.J.; Simmie, J.M. A jet-stirred reactor and kinetic modeling study of ethyl propanoate oxidation. *Combust. Flame* **2009**, *156*, 250–260. [CrossRef]
10. Zhang, J.; Pan, L.; Mo, J.; Gong, J.; Huang, Z.; Law, C.K. A shock tube and kinetic modeling study of n-butanol oxidation. *Combust. Flame* **2013**, *160*, 1541–1549. [CrossRef]
11. Richter, H.; Howard, J.B. Formation of polycyclic aromatic hydrocarbons and their growth to soot—a review of chemical reaction pathways. *Prog. Energy Combust. Sci.* **2000**, *26*, 565–608. [CrossRef]
12. Grana, R.; Frassoldati, A.; Faravelli, T.; Niemann, U.; Ranzi, E.; Seiser, R.; Cattolica, R.; Seshadri, K. An experimental and kinetic modeling study of combustion of isomers of butanol. *Combust. Flame* **2010**, *157*, 2137–2154. [CrossRef]
13. Yoshiaki, H.; Tsuyoshi, K.; Masao, S. A Shock-tube Investigation of Ignition in Ethylene–Oxygen–Argon Mixtures. *Bull. Chem. Soc. Jpn.* **1974**, *47*, 2166–2170.
14. Brown, C.J.; Thomas, G.O. Experimental studies of shock-induced ignition and transition to detonation in ethylene and propane mixtures. *Combust. Flame* **1999**, *117*, 861–870. [CrossRef]
15. Horning, D.C. *A Study of the High-temperature Autoignition and Thermal Decomposition of Hydrocarbons*; Stanford University: Stanford, CA, USA, 2001.

16. Colket, M.B., III; Spadaccini, L.J. Scramjet Fuels Autoignition Study. *J. Propuls. Power* **2001**, *17*, 315–323. [[CrossRef](#)]
17. Kalitan, D.M.; Hall, J.M.; Petersen, E.L. Ignition and Oxidation of Ethylene-Oxygen-Diluent Mixtures with and Without Silane. *J. Propuls. Power* **2005**, *21*, 1045–1056. [[CrossRef](#)]
18. Kumar, K.; Mittal, G.; Sung, C.-J.; Law, C.K. An experimental investigation of ethylene/O<sub>2</sub>/diluent mixtures: Laminar flame speeds with preheat and ignition delays at high pressures. *Combust. Flame* **2008**, *153*, 343–354. [[CrossRef](#)]
19. Penyazkov, O.G.; Sevrouk, K.L.; Tangirala, V.; Joshi, N. High-pressure ethylene oxidation behind reflected shock waves. *Proc. Combust. Inst.* **2009**, *32*, 2421–2428. [[CrossRef](#)]
20. Tereza, A.M.; Slutskii, V.G.; Severin, E.S. Autoignition of ethylene in shock waves. *Russ. J. Phys. Chem. B* **2010**, *4*, 475–485. [[CrossRef](#)]
21. Saxena, S.; Kahandawala, M.S.P.; Sidhu, S.S. A shock tube study of ignition delay in the combustion of ethylene. *Combust. Flame* **2011**, *158*, 1019–1031. [[CrossRef](#)]
22. Davidson, D.; Ren, W.; Hanson, R. Experimental Database for Development of a HiFiRE JP-7 Surrogate Fuel Mechanism. In Proceedings of the 50th AIAA Aerospace Sciences Meeting including the New Horizons Forum and Aerospace Exposition, Nashville, TN, USA, 9–12 January 2012; American Institute of Aeronautics and Astronautics: Reston, VA, USA, 2012.
23. Kopp, M.M.; Donato, N.S.; Petersen, E.L.; Metcalfe, W.K.; Burke, S.M.; Curran, H.J. Oxidation of Ethylene–Air Mixtures at Elevated Pressures, Part 1: Experimental Results. *J. Propuls. Power* **2014**, *30*, 790–798. [[CrossRef](#)]
24. Kopp, M.M.; Petersen, E.L.; Metcalfe, W.K.; Burke, S.M.; Curran, H.J. Oxidation of Ethylene—Air Mixtures at Elevated Pressures, Part 2: Chemical Kinetics. *J. Propuls. Power* **2014**, *30*, 799–811. [[CrossRef](#)]
25. Mathieu, O.; Goulier, J.; Gourmel, F.; Mannan, M.S.; Chaumeix, N.; Petersen, E.L. Experimental study of the effect of CF<sub>3</sub>I addition on the ignition delay time and laminar flame speed of methane, ethylene, and propane. *Proc. Combust. Inst.* **2015**, *35*, 2731–2739. [[CrossRef](#)]
26. Xiong, X.-H.; Ding, Y.-J.; Cao, X.-B.; Peng, Z.-M.; Li, Y.-H. Ethylene Oxidation Experimental Study and Kinetic Mechanism Analysis Based on Shock Tube. *Acta Phys. Chim. Sin.* **2016**, *32*, 1416–1423. [[CrossRef](#)]
27. Shao, J.; Davidson, D.F.; Hanson, R.K. A shock tube study of ignition delay times in diluted methane, ethylene, propene and their blends at elevated pressures. *Fuel* **2018**, *225*, 370–380. [[CrossRef](#)]
28. Baigmohammadi, M.; Patel, V.; Martinez, S.; Panigrahy, S.; Ramalingam, A.; Burke, U.; Somers, K.P.; Heufer, K.A.; Pekalski, A.; Curran, H.J. A Comprehensive Experimental and Simulation Study of Ignition Delay Time Characteristics of Single Fuel C<sub>1</sub>–C<sub>2</sub> Hydrocarbons over a Wide Range of Temperatures, Pressures, Equivalence Ratios, and Dilutions. *Energy Fuels* **2020**, *34*, 3755–3771. [[CrossRef](#)]
29. Dong, S.; Zhang, K.; Senecal, P.K.; Kukkadapu, G.; Wagnon, S.W.; Barrett, S.; Lokachari, N.; Panigrahy, S.; Pitz, W.J.; Curran, H.J. A comparative reactivity study of 1-alkene fuels from ethylene to 1-heptene. *Proc. Combust. Inst.* **2021**, *38*, 611–619. [[CrossRef](#)]
30. Wan, Z.; Zheng, Z.; Wang, Y.; Zhang, D.; Li, P.; Zhang, C. A Shock Tube Study of Ethylene/Air Ignition Characteristics over a Wide Temperature Range. *Combust. Sci. Technol.* **2020**, *192*, 2297–2305. [[CrossRef](#)]
31. Xiong, X.; Lv, Z.; Tan, H.; Peng, Z.; Ding, Y. Shock tube evaluation on C<sub>2</sub>H<sub>4</sub> ignition delay differences among N<sub>2</sub>, Ar, He, CO<sub>2</sub> diluent gases. *J. Energy Inst.* **2020**, *93*, 1271–1277. [[CrossRef](#)]
32. Yang, M.; Wan, Z.; Tan, N.; Zhang, C.; Wang, J.; Li, X. An experimental and modeling study of ethylene–air combustion over a wide temperature range. *Combust. Flame* **2020**, *221*, 20–40. [[CrossRef](#)]
33. Marinov, N.M.; Pitz, W.J.; Westbrook, C.K.; Vincitore, A.M.; Castaldi, M.J.; Senkan, S.M.; Melius, C.F. Aromatic and Polycyclic Aromatic Hydrocarbon Formation in a Laminar Premixed n-Butane Flame. *Combust. Flame* **1998**, *114*, 192–213. [[CrossRef](#)]
34. Burcat, A.; Radhakrishnan, K. High temperature oxidation of propene. *Combust. Flame* **1985**, *60*, 157–169. [[CrossRef](#)]
35. Qin, Z.; Yang, H.; Gardiner, W.C. Measurement and modeling of shock-tube ignition delay for propene. *Combust. Flame* **2001**, *124*, 246–254. [[CrossRef](#)]
36. Heyberger, B.; Belmekki, N.; Conraud, V.; Glaude, P.-A.; Fournet, R.; Battin-Leclerc, F. Oxidation of small alkenes at high temperature. *Int. J. Chem. Kinet.* **2002**, *34*, 666–677. [[CrossRef](#)]
37. Leon, L.; Goos, E.; Klauer, C.; Seidel, L.; Zeuch, T. Evaluation of the influence of thermodynamic data for propane and propene ignition delay time. In Proceedings of the 6th European Combustion Meeting (ECM), Lund, Sweden, 25–28 June 2013.
38. Burke, S.M.; Metcalfe, W.; Herbstein, O.; Battin-Leclerc, F.; Haas, F.M.; Santner, J.; Dryer, F.L.; Curran, H.J. An experimental and modeling study of propene oxidation. Part 1: Speciation measurements in jet-stirred and flow reactors. *Combust. Flame* **2014**, *161*, 2765–2784. [[CrossRef](#)]
39. Burke, S.M.; Burke, U.; Mc Donagh, R.; Mathieu, O.; Osorio, I.; Keese, C.; Morones, A.; Petersen, E.L.; Wang, W.; DeVerter, T.A.; et al. An experimental and modeling study of propene oxidation. Part 2: Ignition delay time and flame speed measurements. *Combust. Flame* **2015**, *162*, 296–314. [[CrossRef](#)]
40. Westbrook, C.K.; Pitz, W.J. A Comprehensive Chemical Kinetic Reaction Mechanism for Oxidation and Pyrolysis of Propane and Propene. *Combust. Sci. Technol.* **1984**, *37*, 117–152. [[CrossRef](#)]
41. Dagaut, P.; Cathonnet, M.; Boettner, J.C. Experimental study and kinetic modeling of propene oxidation in a jet stirred flow reactor. *J. Phys. Chem.* **1988**, *92*, 661–671. [[CrossRef](#)]
42. Pan, L.; Hu, E.; Zhang, J.; Tian, Z.; Li, X.; Huang, Z. A high pressure shock tube study of 1-butene oxidation and its comparison with n-butane and alkenes. *Fuel* **2015**, *157*, 21–27. [[CrossRef](#)]

43. Li, Y.; Zhou, C.-W.; Curran, H.J. An extensive experimental and modeling study of 1-butene oxidation. *Combust. Flame* **2017**, *181*, 198–213. [CrossRef]
44. Kikui, S.; Nakamura, H.; Tezuka, T.; Hasegawa, S.; Maruta, K. Study on combustion and ignition characteristics of ethylene, propylene, 1-butene and 1-pentene in a micro flow reactor with a controlled temperature profile. *Combust. Flame* **2016**, *163*, 209–219. [CrossRef]
45. Li, Y.; Zhou, C.-W.; Somers, K.P.; Zhang, K.; Curran, H.J. The oxidation of 2-butene: A high pressure ignition delay, kinetic modeling study and reactivity comparison with isobutene and 1-butene. *Proc. Combust. Inst.* **2017**, *36*, 403–411. [CrossRef]
46. Jach, A.; Rudy, W.; Pękalski, A.; Teodorczyk, A. Assessment of detailed reaction mechanisms for reproduction of ignition delay times of C<sub>2</sub>–C<sub>6</sub> alkenes and acetylene. *Combust. Flame* **2019**, *206*, 37–50. [CrossRef]
47. Nagaraja, S.S.; Liang, J.; Dong, S.; Panigrahy, S.; Sahu, A.; Kukkadapu, G.; Wagnon, S.W.; Pitz, W.J.; Curran, H.J. A hierarchical single-pulse shock tube pyrolysis study of C<sub>2</sub>–C<sub>6</sub> 1-alkenes. *Combust. Flame* **2020**, *219*, 456–466. [CrossRef]
48. Zhang, Y.; Huang, Z.; Wei, L.; Zhang, J.; Law, C.K. Experimental and modeling study on ignition delays of lean mixtures of methane, hydrogen, oxygen, and argon at elevated pressures. *Combust. Flame* **2012**, *159*, 918–931. [CrossRef]
49. Chris, M. Gaseq Version 0.79. Available online: <http://www.gaseq.co.uk> (accessed on 21 January 2018).
50. Deng, F.; Yang, F.; Zhang, P.; Pan, Y.; Bugler, J.; Curran, H.J.; Zhang, Y.; Huang, Z. Towards a kinetic understanding of the NO<sub>x</sub> promoting-effect on ignition of coalbed methane: A case study of methane/nitrogen dioxide mixtures. *Fuel* **2016**, *181*, 188–198. [CrossRef]
51. Sun, W.; Huang, W.; Qin, X.; Deng, Y.; Kang, Y.; Peng, W.; Zhang, Y.; Huang, Z. Water impact on the auto-ignition of kerosene/air mixtures under combustor relevant conditions. *Fuel* **2020**, *267*, 117184. [CrossRef]
52. Petersen, E.L.; Rickard, M.J.A.; Crofton, M.W.; Abbey, E.D.; Traum, M.J.; Kalitan, D.M. A facility for gas- and condensed-phase measurements behind shock waves. *Meas. Sci. Technol.* **2005**, *16*, 1716–1729. [CrossRef]
53. CHMEKIN-PRO; Reaction Design Inc.: San Diego, CA, USA; Available online: <https://www.Ansys.com/> (accessed on 25 September 2017).
54. Deng, F.; Yang, F.; Zhang, P.; Pan, Y.; Zhang, Y.; Huang, Z. Ignition delay time and chemical kinetic study of methane and nitrous oxide mixtures at high temperatures. *Energy Fuels* **2016**, *30*, 1415–1427. [CrossRef]
55. Chaos, M.; Dryer, F.L. Chemical-kinetic modeling of ignition delay: Considerations in interpreting shock tube data. *Int. J. Chem. Kinet.* **2010**, *42*, 143–150. [CrossRef]
56. Bross, B.R.D.H. Active Thermochemical Tables (ATcT) values based on ver. 1.122p of the Thermochemical Network. 2020. Available online: <ATcT.anl.gov> (accessed on 8 March 2020).
57. Baigmohammadi, M.; Patel, V.; Nagaraja, S.; Ramalingam, A.; Martinez, S.; Panigrahy, S.; Mohamed, A.A.E.-S.; Somers, K.P.; Burke, U.; Heufer, K.A.; et al. Comprehensive experimental and simulation study of the ignition delay time characteristics of binary blended methane, ethane, and ethylene over a wide range of temperature, pressure, equivalence ratio, and dilution. *Energy Fuels* **2020**, *34*, 8808–8823. [CrossRef]
58. Lokachari, N.; Panigrahy, S.; Kukkadapu, G.; Kim, G.; Vasu, S.S.; Pitz, W.J.; Curran, H.J. The influence of iso-butene kinetics on the reactivity of di-isobutylene and iso-octane. *Combust. Flame* **2020**, *222*, 186–195. [CrossRef]
59. Nagaraja, S.S.; Power, J.; Kukkadapu, G.; Dong, S.; Wagnon, S.W.; Pitz, W.J.; Curran, H.J. A single pulse shock tube study of pentene isomer pyrolysis. *Proc. Combust. Inst.* **2020**, *38*, 881–889. [CrossRef]
60. Panigrahy, S.; Liang, J.; Nagaraja, S.S.; Zuo, Z.; Kim, G.; Dong, S.; Kukkadapu, G.; Pitz, W.J.; Vasu, S.S.; Curran, H.J. A comprehensive experimental and improved kinetic modeling study on the pyrolysis and oxidation of propyne. *Proc. Combust. Inst.* **2020**, *38*, 479–488. [CrossRef]
61. Dong, S.; Zhang, K.; Ninnemann, E.M.; Najjar, A.; Kukkadapu, G.; Baker, J.; Arafin, F.; Wang, Z.; Pitz, W.J.; Vasu, S.S.; et al. A comprehensive experimental and kinetic modeling study of 1- and 2-pentene. *Combust. Flame* **2021**, *223*, 166–180. [CrossRef]
62. Ramalingam, A.; Panigrahy, S.; Fenard, Y.; Curran, H.; Heufer, K.A. A chemical kinetic perspective on the low-temperature oxidation of propane/propene mixtures through experiments and kinetic analyses. *Combust. Flame* **2021**, *223*, 361–375. [CrossRef]
63. Wu, Y.; Panigrahy, S.; Sahu, A.B.; Bariki, C.; Beeckmann, J.; Liang, J.; Mohamed, A.A.; Dong, S.; Tang, C.; Pitsch, H.; et al. Understanding the antagonistic effect of methanol as a component in surrogate fuel models: A case study of methanol/n-heptane mixtures. *Combust. Flame* **2021**, *226*, 229–242. [CrossRef]
64. Kéromnès, A.; Metcalfe, W.K.; Heufer, K.A.; Donohoe, N.; Das, A.K.; Sung, C.-J.; Herzler, J.; Naumann, C.; Griebel, P.; Mathieu, O.; et al. An experimental and detailed chemical kinetic modeling study of hydrogen and syngas mixture oxidation at elevated pressures. *Combust. Flame* **2013**, *160*, 995–1011. [CrossRef]
65. Zhou, C.-W.; Li, Y.; O'Connor, E.; Somers, K.P.; Thion, S.; Keese, C.; Mathieu, O.; Petersen, E.L.; DeVerter, T.A.; Oehlschlaeger, M.A.; et al. A comprehensive experimental and modeling study of isobutene oxidation. *Combust. Flame* **2016**, *167*, 353–379. [CrossRef]
66. Ranzi, E.; Frassoldati, A.; Stagni, A.; Pelucchi, M.; Cuoci, A.; Faravelli, T. Reduced Kinetic Schemes of Complex Reaction Systems: Fossil and Biomass-Derived Transportation Fuels. *Int. J. Chem. Kinet.* **2014**, *46*, 512–542. [CrossRef]
67. Pejpichestakul, W.; Ranzi, E.; Pelucchi, M.; Frassoldati, A.; Cuoci, A.; Parente, A.; Parente, A.; Faravelli, T. Examination of a soot model in premixed laminar flames at fuel-rich conditions. *Proc. Combust. Inst.* **2019**, *37*, 1013–1021. [CrossRef]
68. Chemical-Kinetic Mechanisms for Combustion Applications. Available online: <http://combustion.ucsd.edu> (accessed on 7 December 2020).

69. Wang, H.; Dames, E.; Sirjean, B.; Sheen, D.A.; Tango, R.; Violi, A.; Lai, J.Y.W.; Egolfopoulos, F.N.; Davidson, D.F.; Hanson, R.K.; et al. A high-temperature chemical kinetic model of n-alkane (up to n-dodecane), cyclohexane, and methyl-, ethyl-, n-propyl and n-butyl-cyclohexane oxidation at high temperatures, JetSurF version 2.0. 19 September 2010. Available online: <http://melchior.usc.edu/JetSurF/JetSurF2.0> (accessed on 15 November 2020).
70. Konnov, A.A. Implementation of the NCN pathway of prompt-NO formation in the detailed reaction mechanism. *Combust. Flame* **2009**, *156*, 2093–2105. [[CrossRef](#)]
71. Wang, H.; You, X.; Joshi, A.V.; Davis, S.G.; Laskin, A.; Egolfopoulos, F.; Law, C.K. USC Mech Version II. High-Temperature Combustion Reaction Model of H<sub>2</sub>/CO/C<sub>1</sub>-C<sub>4</sub> Compounds. May 2007. Available online: [http://ignis.usc.edu/USC\\_Mech\\_II.htm](http://ignis.usc.edu/USC_Mech_II.htm) (accessed on 14 December 2020).
72. Lopez, J.G.; Rasmussen, C.L.; Alzueta, M.U.; Gao, Y.; Marshall, P.; Glarborg, P. Experimental and kinetic modeling study of C<sub>2</sub>H<sub>4</sub> oxidation at high pressure. *Proc. Combust. Inst.* **2009**, *32*, 367–375. [[CrossRef](#)]